POLITECNICO DI TORINO

Laurea Magistrale in Ingegneria Aerospaziale

Master Thesis

Eurocargo CNG E6 Exhaust System: Acoustic Simulation and SNGR Approach by ACTRAN

Supervisors:

prof. Renzo ARINA

prof. Federico MILLO

ing. Benedetta PEIRETTI PARADISI

Candidate:

Lorenzo GARIBALDI

April 2021

Eurocargo CNG E6 Exhaust System: Acoustic Simulation and SNGR Approach by ACTRAN

Lorenzo Garibaldi

8 April 2021

ABSTRACT

The study of noise generated by the exhaust system is a fundamental step in the project of a truck. For this class of vehicles such system is one of the major sources of noise and many configurations are tested in order to reduce the amount of perceived noise, as well as improve global performance. This work aims to estimate the noise generated by the exhaust system of a truck in its surrounding area through the specific software for acoustic and aeroacoustic simulations MSC Actran. In order to achieve this result, the SNGR method is used to determine the acoustic sources at the exhaust outlet from a steady state CFD simulation, and then noise is propagated in far field through the Lighthill formulation. Downstream of this analysis, it is shown the difference in terms of generated noise between the baseline configuration of the terminal part of the exhaust system, the diffusor, and its modified version, characterized by the addition of a perforated plate at the inlet.

CONTENTS

LIST OF FIGURES

LIST OF TABLES

1. INTRODUCTION: HYBRID METHODS AND SNGR APPROACH

The project of a truck involves as a fundamental step the study of the noise generated by the exhaust system. Such system certainly represents one of the main contributions to noise on the vehicle and different configurations are tested with the aim of reducing the acoustic disturbance and improving the truck's global performance. The goal of this work is to estimate the noise generated by the exhaust system of a truck in its surrounding area (in particular in the space between the floor and truck's down side) through a specific software for acoustic, vibroacoustic and aeroacoustic simulations developed by *Free Field Technologies* company, MSC Actran.
Actually, the acoustic analysis only takes into account the terminal part of the exhaust system, the diffusor, in two different configurations: the baseline design and design with perforated plate. The latter could potentially be a solution for noise reduction to be verified through numerical analysis.
A *hybrid approach* is used during the simulation, that means the problem is split into two parts: the computation of noise sources in the diffusor, starting from a previous CFD analysis performed on the entire exhaust system, and acoustic propagation in the external environment. Both parts are performed by Actran: reconstruction of acoustic sources in frequency domain is obtained through Actran iCFD utility, while noise propagation involves an Actran *Direct Frequency Response* analysis on the whole acoustic domain.
Hybrid methods have been established as practical methods for fast and accurate aeroacoustic computations at low Mach numbers. Unlike direct methods, in which both the flow and the acoustic propagation are solved with CFD code, they involve two different steps: sound generation and sound propagation. Indeed, hybrid models are defined such that flow and acoustic propagation are modelled separately. This separation comes from the difficulties met during the simulation of flow noise problems: the large disparity between energy in the flow and acoustic radiated energy, the difference between the size of eddies in turbulent flow and wavelength of generated acoustic sound, the need to preserve the multipole structure of acoustic sources, the boundary treatment in simulation involving unbounded domains and the nonlinear effects in high speed turbulent flow. Hybrid schemes use aeroacoustic analogies, such as Lighthill analogy, to perform acoustic propagation and to separate this phase from flow computation. This implies a variable computational grid over the flow field: near walls is finer to resolve boundary

layers and is coarsened towards outflow boundaries. Moreover, in the acoustic region the grid has to transport sound waves, so the grid size needs to be uniform all over the computational domain [1]. Beside this, mean flow mesh and acoustic mesh need to be correctly coupled through an interpolation scheme that has to minimize the interpolation errors and satisfy the energy conservation among the two regions. However, the *fundamental hypothesis* underlying the hybrid approach is that the effect of the acoustic field on the flow field is neglected, that is mean flow generates acoustic waves without retroactive effect of the waves on the flow field.

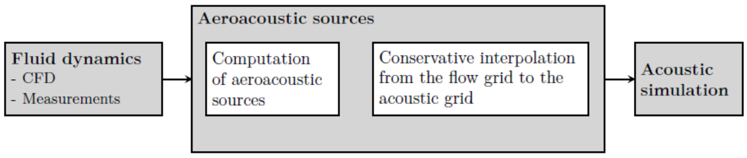

Fig. 1.1: Hybrid aeroacoustic workflow [2]

Hybrid schemes find several applications also because they allow to evaluate the sound radiation with a low computational cost. Moreover, they are more affordable than direct methods in terms of computing power and time and are often the only methods applicable in complex configurations. On the other side, they can lack information on the interactions between the aerodynamic and acoustic fields: refraction effects by the mean flow are incompletely, or even not at all, computed, as well as potential couplings between the two fields [5]. In hybrid methods unsteady near-field flow may be simulated using LES or DES solver and then acoustic analogy gives the propagation of sound into far field using near-field sound sources as input. A typical case is a jet-nozzle configuration, which is simulated using LES in the near-field and extraction of acoustic far-field is conducted through a FW-H integral method [3]. Also IDDES (Improved Delayed Detached Eddy Simulation) may be adopted to simulate unsteady flow field before the evaluation of the sources for the acoustic propagation ([4], a numerical study of aerodynamic and acoustic installation effects of an automotive cooling module).
However, in this study flow results and creation of the model came from a previous *steady* CFD analysis by STAR-CCM+, where a RANS (Reynolds Averaged Navier-Stokes) simulation was performed. In RANS method, flow variables are decomposed into a time-averaged term and a fluctuating quantity, with the latter being modeled basing on the properties of flow turbulence. The method itself includes several approximations, but it is also the least expensive from the computational point of view. The next step was to obtain an unsteady velocity field from the steady analysis and then compute

the acoustic sources. This has been done through SNGR formulation. SNGR (*Stochastic Noise Generation and Radiation*) is a computational aeroacoustic method that allows to synthetize an unsteady flow field for mapping the acoustic sources starting from a steady RANS computation. An unsteady analysis using CFD code (DNS or LES) has some limitations, indeed: the size of the whole acoustic domain is not suitable for sources computation, the cost of simulations is high and not all frequencies are reached.
Through SNGR method it is possible to identify and circumscribe noise sources regions reducing CFD computational cost and at the same time to recover high frequency flow contents. SNGR is characterized by some *basic assumptions*: the flow is incompressible and at low Mach number, the reconstructed turbulence is homogeneous and isotropic, acoustic sources are spatially uncorrelated and velocity spectrum depends on local turbulent kinetic energy (TKE). RANS numerical simulations with $K - \epsilon$ turbulence model provide mean flow variables (velocity, density and pressure), turbulent kinetic energy (K) and dissipation rate (ϵ), that first can be used to derive the turbulent energy field through Von Karman - Pao spectrum (fig. 1.2) or similar formulations, and then the turbulent velocity field [6].

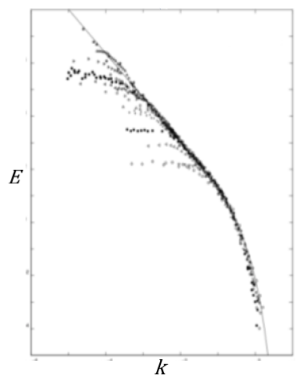

Fig. 1.2: Von Karman - Pao spectrum

Von Karman - Pao spectrum is a class of turbulent spectrum through which it is possible to extract the turbulent energy having RANS results as input and selecting a certain number of frequency modes (k). Such turbulent energy $E(k)$ is then used, according to SNGR, to build the instantaneous turbulent velocity, that is given by the following expression:

$$\vec{v}' = \sum_{\lambda} \sqrt{E(k_\lambda)\Delta k_\lambda} \cos\left(k_\lambda \vec{l}_\lambda (\vec{x} - \vec{u}t) - \omega_\lambda t - \phi\right)\vec{\sigma}$$

where some terms in brackets ($\vec{l}_\lambda, \phi$) are random numbers generators, to put in evidence the stochastic approach of the method.

Hence, acoustic sources are created because in Lighthill formulation the volume source term at right hand side is completely available using SNGR method. In fact, turbulent velocity field obtained earlier appear in the expression of the volume term as velocity components v_i and v_j:

$$\int_V \frac{\partial N_a}{\partial x_i} \frac{\partial \rho v_i v_j}{\partial x_j} dV \tag{1.1}$$

The first factor contained in the integral is known because of the definition of the acoustic mesh. As we have already mentioned, the analysis source computation is directly performed in frequency domain, unlike methods having unsteady simulations as input.
In other applications a system of linearized Euler equations (LEE) is used to compute the acoustic propagation instead of the classical wave equation, and also for this case the first step is the knowledge of the turbulent velocity field. For example, it is the case of studies that involve two-dimensional ducts obstructed by an obstacle, such as diaphragms, where the classical approach to use the free-space Green's function to solve the wave equation is not applicable because of the flow's rotationality and the confined configuration of the system [7]. Here a propagation system of first-order differential equations is solved using values of the mean flow field as coefficients and the acoustic source term is calculated from the synthetized turbulent field. As usual, the space-time stochastic turbulent velocity field is generated as a sum of random Fourier modes. Other studies have put in evidence the relationship between the size of the source region and SNGR model itself [8]. As the first one has a direct impact on time and memory requirements during the stochastic reconstruction of turbulent velocity components, a cut-off coefficient may be defined. It determines the size of the source region by considering only grid points with turbulent kinetic energy greater than the product of the maximum TKE and the coefficient itself. For this reason, memory requirements and time costs in SNGR decrease significantly with increasing of cut-off coefficient, which can be used as a control parameter in sources reconstruction process. In most cases the best approach is to set the largest possible value of the coefficient fulfilling at the same time the required accuracy.

About the general organization of this work, the next chapter deals with the description of the truck's exhaust system and, considering the generated flow, main results of the CFD analysis will be shown. The third chapter handles the acoustic analysis by means of Actran, that leads to the creation of acoustic maps simulating noise propagation in far field; in this part the Actran iCFD utility is used to process CFD results and to synthesize the acoustic sources in frequency domain. Finally, in the fourth chapter analysis results (maps and SPL diagrams) will be discussed.

2. EXHAUST SYSTEM AND CFD RESULTS

2.1 Exhaust system presentation

Eurocargo CNG E6 is a product of IVECO company and represents a model of truck that ensures a good level of performance and low consumption in the context of urban transport. The exhaust system of the truck is basically composed by three main parts: a three-way catalyst, the muffler and the diffusor. It is known that in automotive applications catalyst's function is to drastically reduce the amount of pollutants contained in the exhaust gases coming from engine through chemical reactions, before expulsion outside the vehicle. The ejection of gases into the external environment takes place through the diffusor, which is the terminal part of the exhaust system. In this case the diffusor is composed by three parallel ducts departing from the component's inlet at the top.

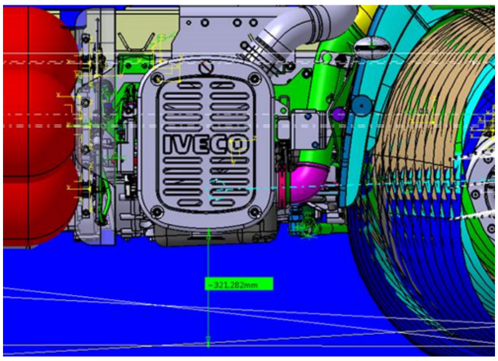

Fig. 2.1: Exhaust system's location on the truck

Figures 2.2, 2.3 and 2.4 show a virtual representation of the exhaust system and its components obtained by means of the software for CFD simulations STAR-CCM+. The depicted red arrows describe the path of exhaust gases coming from engine towards the diffusor outlet, while the spherical region, with center located at the central pipe's outlet, was originally used to simulate free-field condition in the early stages of CFD analysis.

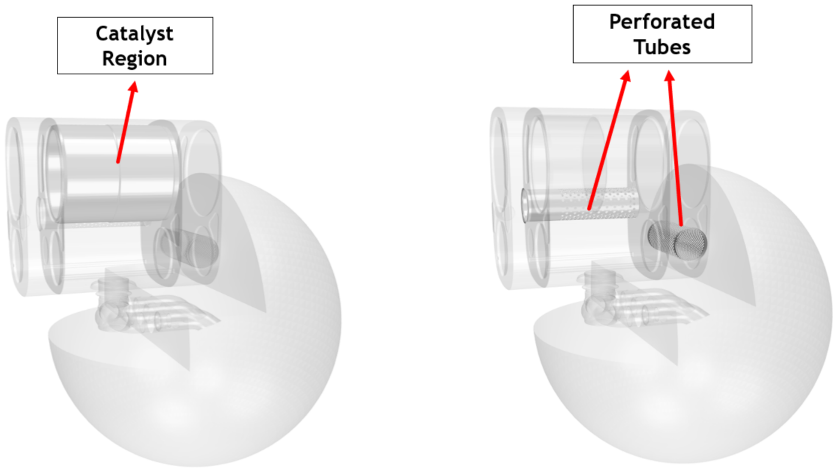

Fig. 2.2: Virtual representation of the system

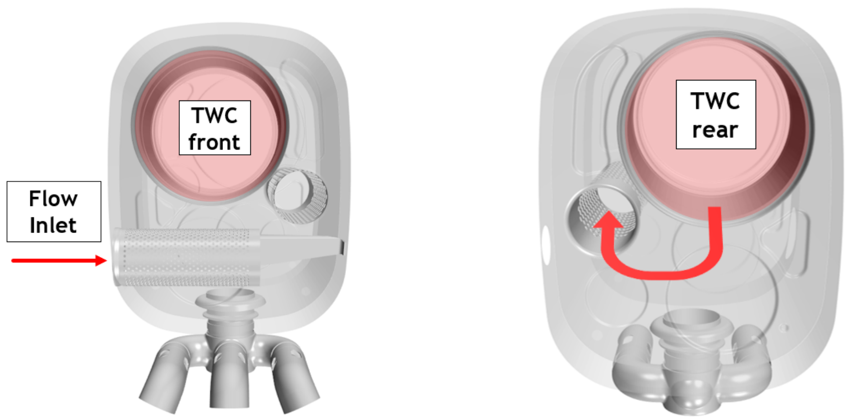

Fig. 2.3: Exhaust system's front and rear views

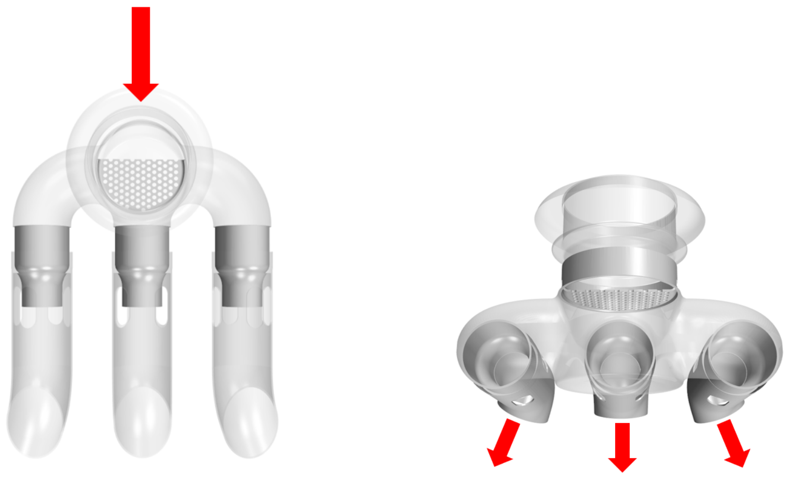

Fig. 2.4: Virtual representation of the diffusor

Tubes conveying exhaust gases towards and outside TWC (Three-Way Catalyst) region have perforated walls in order to dissipate more heat.
Moving back to the objectives of this analysis, the study of noise generated by the flow outcoming from the exhaust system takes into account two different configurations of the diffusor, as we have mentioned in the introduction: the baseline design and the design with a perforated plate at the inlet (fig. 2.5). In both cases we will consider the same boundary conditions at the working point, in terms of thermodynamic and fluid dynamics quantities at the inlet and outlet (see table 2.1).

Fig. 2.5: Diffusor: baseline design and perforated plate design

Inlet Mass Flow Rate	592 kg/h
Inlet Temperature	734 °C
Outlet Pressure	101325 Pa
Outlet Temperature	27 °C

Tab. 2.1: Exhaust system's physical quantities at working point

2.2 CFD analysis results

After the description of the system's basic features, in this section we want to show the main results of the CFD computation performed with STAR-CCM+, since it will be input for the following acoustic analysis. In the CFD analysis, for the *steady state* case, two different versions were considered for the *volume mesh* to describe the system properly: **BD02** and **BD12**.
BD stays for baseline design, which is the first analyzed configuration, and the following numbers identify the mesh type. BD02 is characterized by small elements onto and near the diffusor and coarser elements outside, while BD12 consists of a fine mesh in an inner region including the diffusor and the cone of ejected gases, sourrounded by a middle-sized mesh around the cone (see figures 2.6 - 2.7 and table 2.2 for mesh characteristics).
In a similar way is for the perforated plate configuration, where **PP02** and **PP12** are the corresponding versions. The two different volume mesh set-ups are both taken into account in the computation, and only when Actran analysis results will be avaliable some considerations can be made on which one is the best solution for the acoustic simulation.
Basing only on the CFD results of the *steady state*, we can see from the comparison between BD02 and BD12 a qualitative agreement about the trend of fluid-dynamics variables, but different quantitative results and spatial arrangement. This could potentially affect the distribution and the amplitude of noise sources after the application of SNGR, and as a consequence the acoustic propagation. For this reason, we decide to postpone the complete discussion on the adopted CFD mesh at the end of the whole analysis, depending on the results that will arise from one or the other solution.

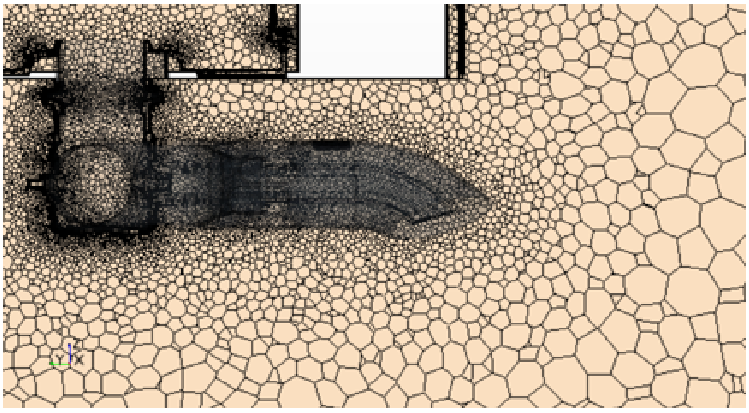

Fig. 2.6: BD02: preliminary set-up for steady state solution

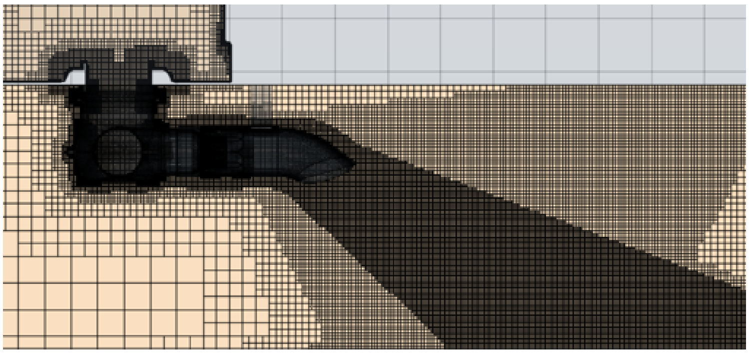

Fig. 2.7: BD12: final RANS set-up for unsteady CFD initialization

	BD02	BD12
base size	8 mm	8 mm
minimum grid size	3 mm	$5 \cdot 10^{-3}$ mm
mesh type	polyhedral mesh	trimmed mesh

Tab. 2.2: BD02 and BD12 characteristics

For now, we just show the main CFD results in terms of velocity and turbulent kinetic energy maps. Figures from 2.8 to 2.15 illustrate distributions on xy and yz plane for BD02 and BD12. In velocity maps the maximum values can be found at the section narrowing in correspondance of the ejectors, where BD02 is characterized by higher velocities than BD12. However, BD02 has lower values in the impingement area of the jets on the bottom of the device. About TKE maps, for both meshes the peak occurs approximately at the pipes intersection and in this case the area with high kinetic energy is more extensive for BD02 than for BD12. Furthermore, unlike what happens for the velocities, from xy view it is possible to notice how the turbulent energy is not equally distributed in the three pipes, but has higher values in the central one.

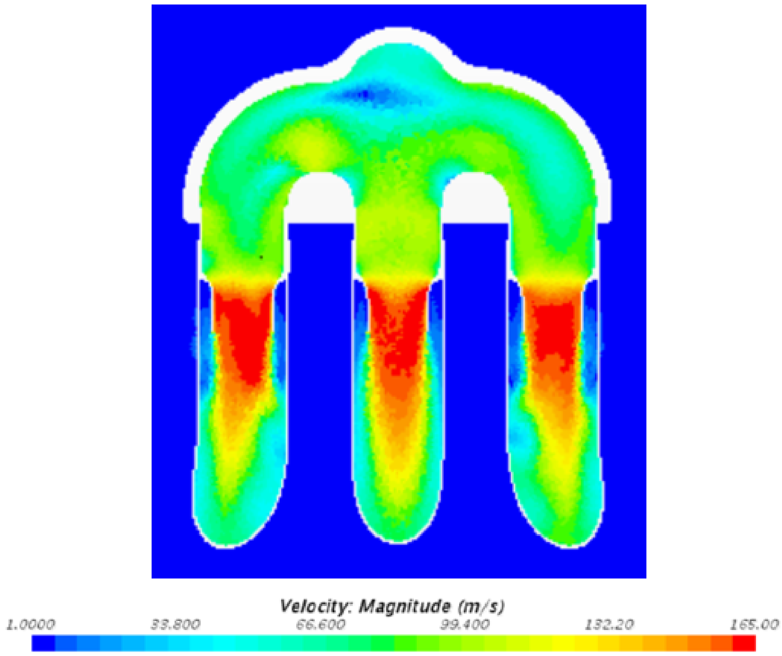

Fig. 2.8: Steady state BD02: velocity magnitude on xy plane

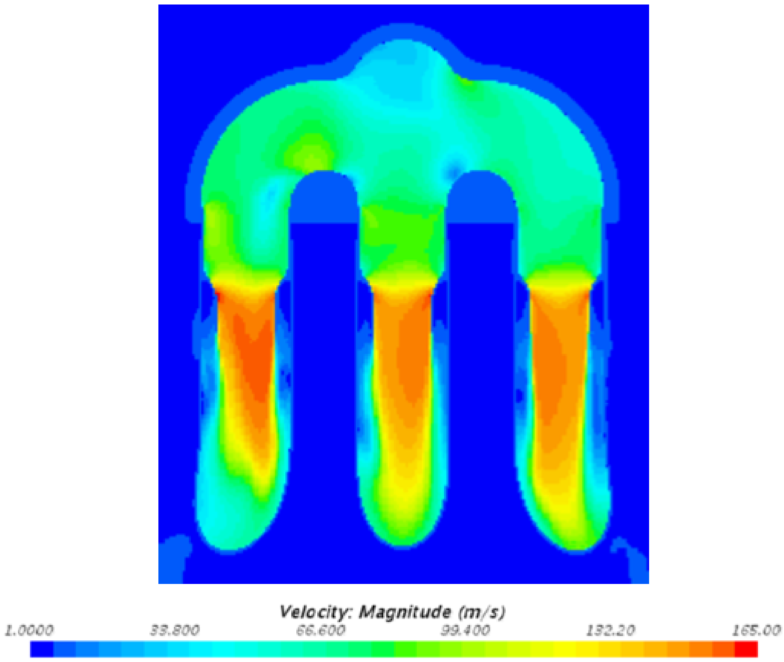

Fig. 2.9: Steady state BD12: velocity magnitude on xy plane

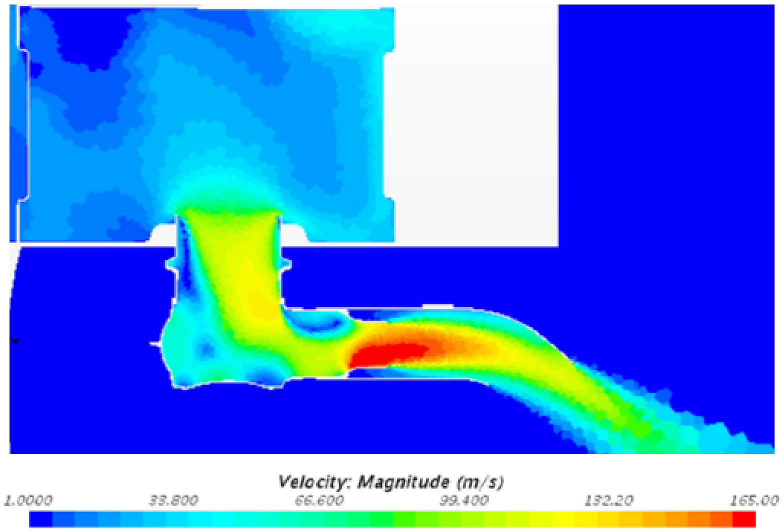

Fig. 2.10: Steady state BD02: velocity magnitude on yz plane

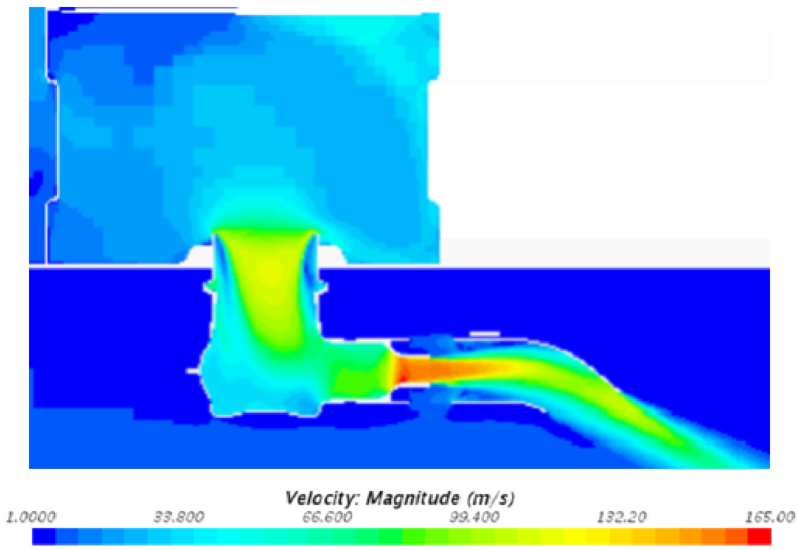

Fig. 2.11: Steady state BD12: velocity magnitude on yz plane

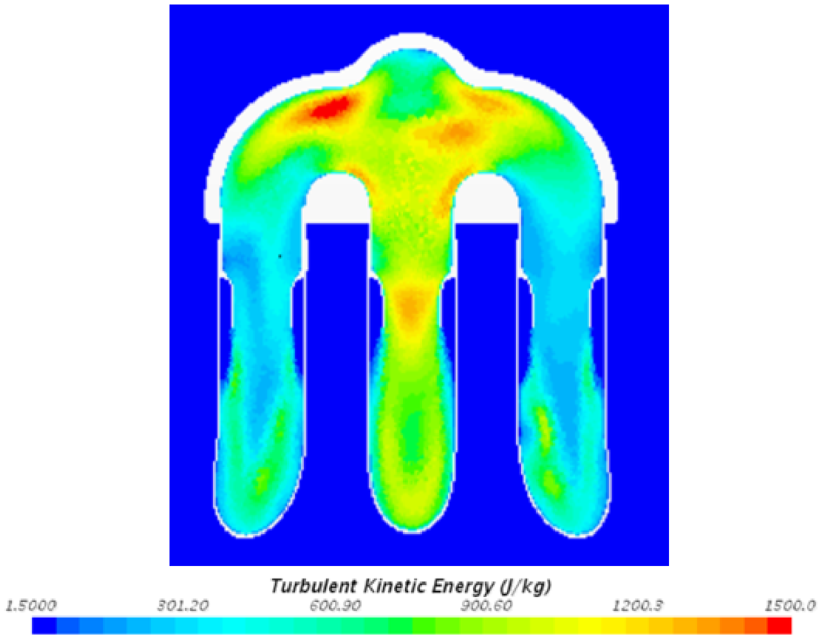

Fig. 2.12: Steady state BD02: turbulent kinetic energy on xy plane

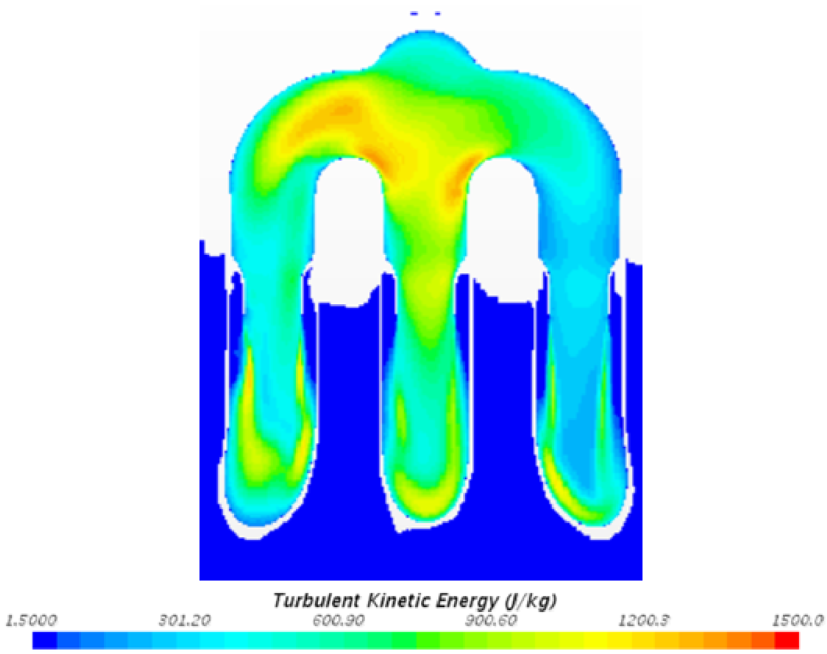

Fig. 2.13: Steady state BD12: turbulent kinetic energy on xy plane

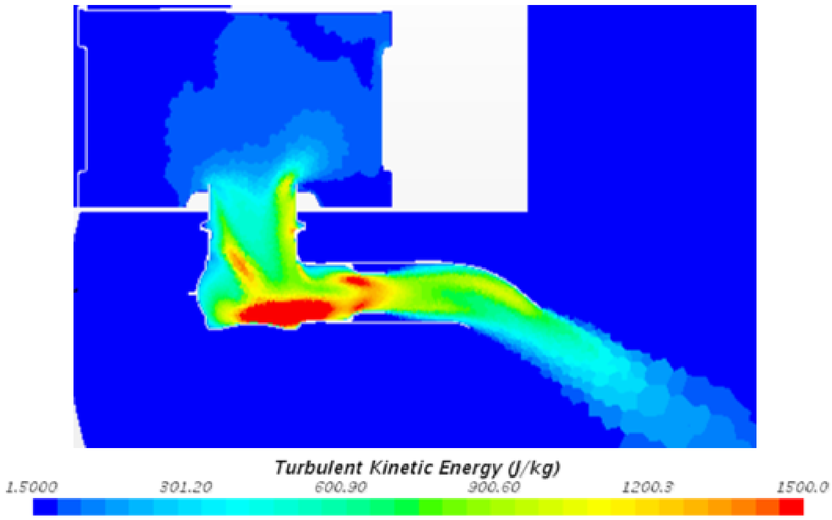

Fig. 2.14: Steady state BD02: turbulent kinetic energy on yz plane

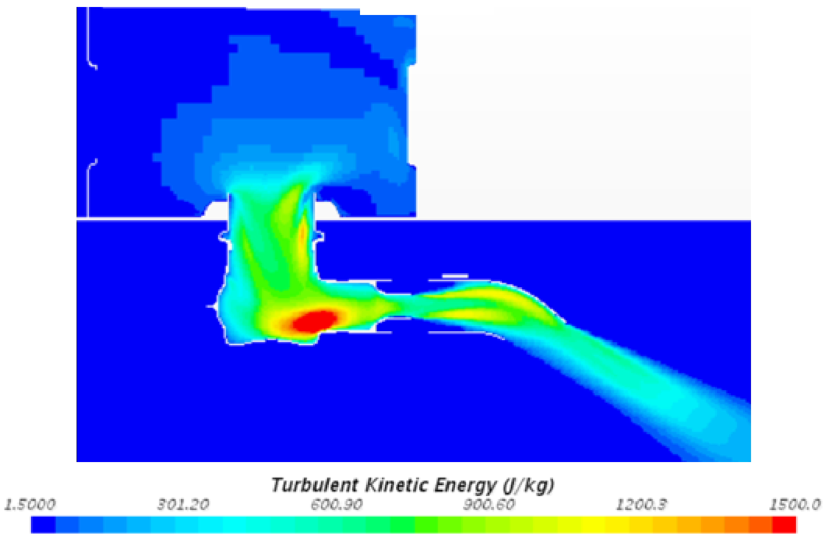

Fig. 2.15: Steady state BD12: turbulent kinetic energy on yz plane

Before going into the analysis of the system, it is first useful to summarize some of ACTRAN's main functions and tools. When we launch the software graphical interface ACTRANVI, the following page pops up.

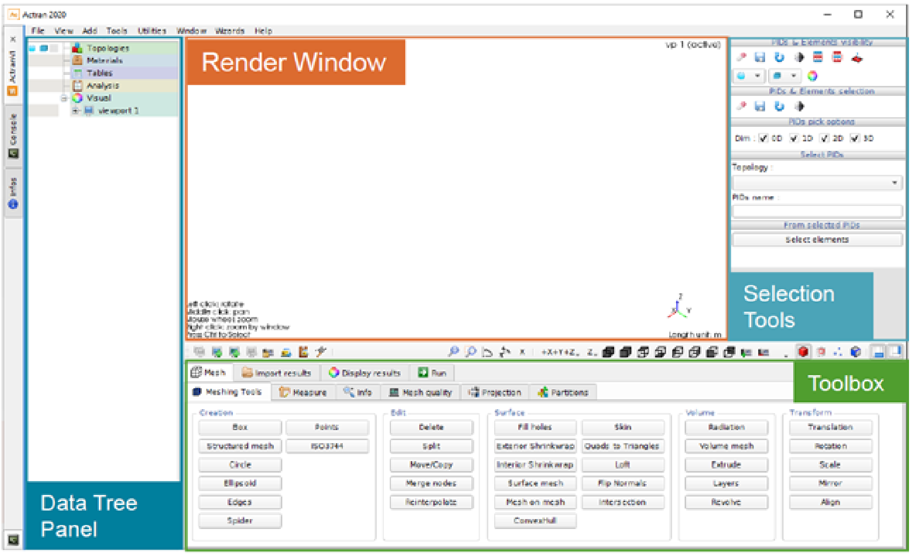

Fig. 3.1: ACTRANVI's main page

Data Tree Panel contains the graphical tree where the different parts of the analysis are displayed: topology, domains, materials, analysis parameters, components, boundary conditions and post-processing are the main branches. In the *Render Window* the geometry of the models involved in the analysis, which is composed by one or more topologies, is shown. It must be said that a topology includes different elements or element sets (an element set is a group of elements with the same characteristics), so it only identifies the geometry of the model. Domains are created to link the geometry with the analysis, instead: a specific option allows to create domains basing on the elements of the topologies, and then every domain is assigned to a component during the analysis set-up. *Toolbox* and *Selection Tools* panels are used to editing the model's geometry and mesh [9] [10]. Now let's start the analysis of the first case, the noise propagation around the truck with the baseline design of the diffusor, with the topology definition.

3.1 Baseline design

3.1.1 Topology

The geometry of the diffusor, which is the only part of the exhaust system considered in the acoustic analysis, was created in STAR-CCM+ because of its complexity and then imported in ACTRAN. The first operation with ACTRAN was to re-mesh the input geometry of the diffusor using a fine mesh with 0.005 m as surface element size (fig. 3.2). The reason for which such a value has been chosen is to describe with sufficient accuracy the geometric variations of the component.

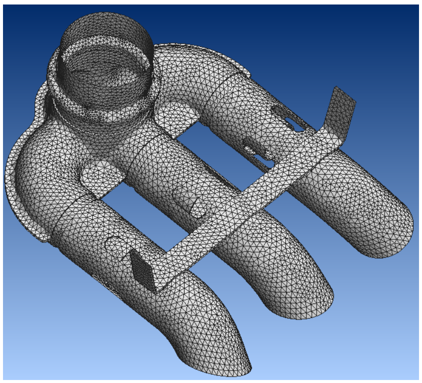

Fig. 3.2: Re-meshed diffusor (baseline configuration)

The next step was the creation of the **source region**, a limited area around the diffusor in which turbulent structures are strong enough to be the main contributions to aeroacoustic noise. According to this definition and taking into account velocity and turbulent energy maps obtained in CFD analysis, several trials have been made to define a suitable region containing the diffusor that did not neglect important turbulent noise sources. The first solution was the creation of a "double" source region, which included a more internal region around the diffuser with a mesh of element size 0.005 m and a more external one with element size 0.015 m connected with the propagation region (see figures 3.3 and 3.4). This new element size, which pertains to surface elements at the boundaries and to volume elements within the different regions, has also been set for the mesh elements of the propagation region. Such value is justified by the maximum frequency set for the acoustic analysis. As we wanted to compute noise propagation up to a frequency of 2000 Hz and the *standard meshing criterion* says to assign at least 8 elements per wavelength in case of *linear elements*, element size is determined by the acoustic wavelength definition $\lambda = c/f$:

$$\lambda_{min} = \frac{c}{f_{max}} = 8 \cdot es \;\Rightarrow\; es = \frac{c}{8 \cdot f_{max}} = \frac{340 \text{ m/s}}{8 \cdot 2000 \text{ Hz}} = 0.021 \text{ m}$$

where c is the speed of sound, f the frequency and es the element size.
As we chose to be conservative in the analysis, we finally took a smaller element size ($es = 0.015$ m) for the meshes of outer source region and propagation region. Anyway, after the visualization of some results, especially sources distribution and pressure maps, it was decided to put this model aside and to consider only a single smaller source region, whose mesh element size is always 0.005 m, surrounded by the propagation region with element size 0.015 m. In fact, we realized that it would have been useless to consider a large source region, as the major contributions to aerodynamic noise are located near the diffusor. In both cases (the old "double" source region model and the new "single" one) the source region was fully included in the truck's downside, even if in the latter case it has been considerably reduced.

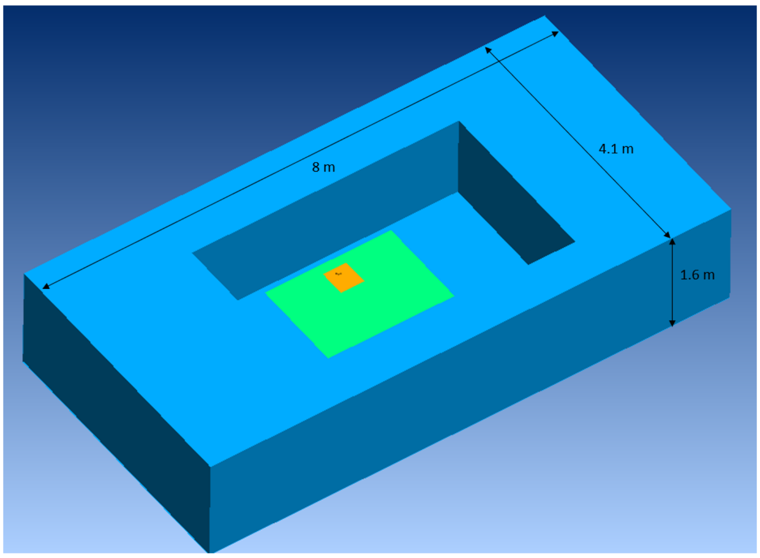

Fig. 3.3: First model with extended propagation region (blue) and "double" source region (orange and green)

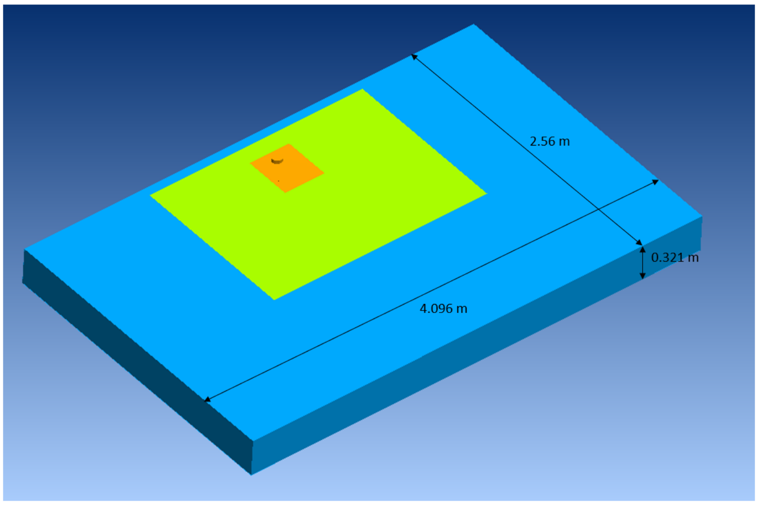

Fig. 3.4: Second model with reduced propagation region (blue) and "double" source region (orange and green)

The **propagation region**, as the name suggests, is a region in which only the acoustic signal propagation is taken into account, and here the turbulence of the ejected flow has so low intensity that it's no more an effective source of noise. The real propagation region is obviously unlimited, but, as we'll see in the next section, by Actran it is possible to simulate a free-field propagation using a finite volume.
Also here for the propagation region, two different configurations were considered. In the first one, the region extended beyond truck's dimensions in the horizontal plane and included acoustic medium near the lateral sides of the vehicle (see figure 3.3). Afterwards, as processor's memory issues came up when launching the acoustic analysis (a big volume with a fine mesh means a large number of elements to resolve), it was decided to reduce the region again to include only the space under the truck (figures 3.4 and 3.5). So the final domain for the acoustic analysis is the one shown in figure 3.5, with source region in orange and propagation region in blue. The lateral boundaries in green are not in contact with any physical walls and they will be used later in the analysis to reproduce an infinite domain. The simulation of a free field acoustic radiation means that the difference between the extended and the reduced version of the propagation region is not relevant for analysis purposes, and in any case results in terms of propagation maps are more appreciable near the source region.

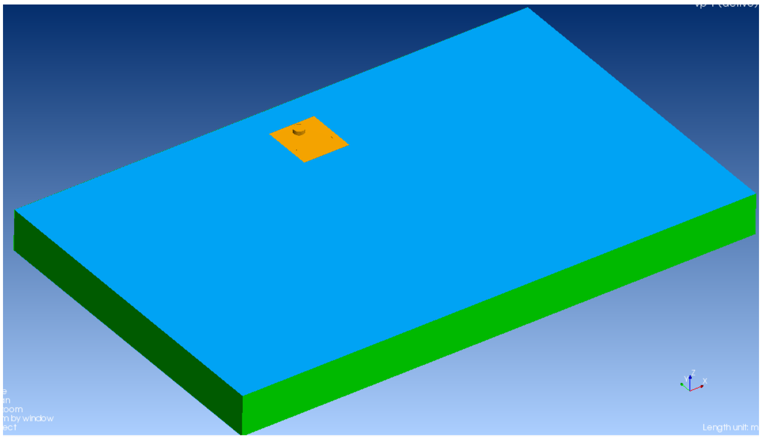

Fig. 3.5: Final model for the acoustic analysis: source region (orange), propagation region (blue) and free field propagation boundaries (green)

In ACTRAN the geometry of the source region was imported from STAR-CCM+ together with the diffuser, and then a *Mesh on mesh* operation was performed to re-mesh the surfaces with triangular elements, setting 0.005 m as element size. After that, a *Volume mesh* operation was made to fill the volume of the source region with tetrahedral and hexahedral elements [1] with element size 0.005 m as well. The propagation region was entirely made in ACTRAN using meshing tools, instead. *Box* and *Surface mesh* were used to create its geometrical shape, and then *Mesh on mesh* and *Volume mesh* were applied to refine the created surface with a 0.015 m element size mesh and to fill the internal volume with elements of the same dimension [11]. Figures 3.6 and 3.7 show some details of the mesh of the created topology in two different planes, xy and yz respectively. It is clearly visible the different size of the elements of source and propagation region.

Source region	0.005 m
Propagation region	0.015 m

Tab. 3.1: Mesh elements size for baseline design

[1] In *Volume mesh* tool, the activation of *Hexacore* option allows to create inner hexaedral elements in order to save time during mesh creation.

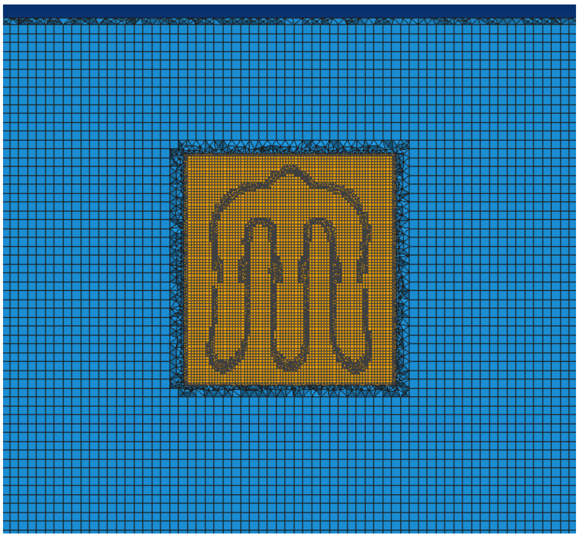

Fig. 3.6: Mesh detail on xy plane

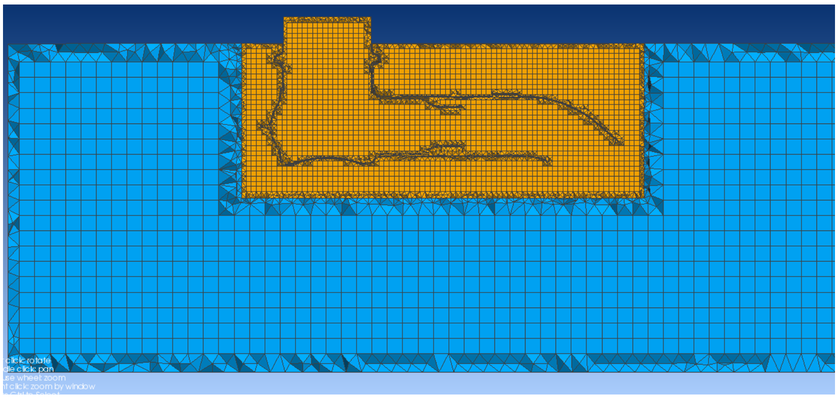

Fig. 3.7: Mesh detail on yz plane

Before moving on to the acoustic analysis, redundant element sets were removed from the topology. It was the case of the bottom and upper sides (fig. 3.8), which represented the floor (the road surface) and the truck's downside respectively, and of the internal surfaces between source and propagation region as well. Such latter interfaces turned out to be critical during the analysis because of the incongruence of border nodes in the first few attempts: a *Merge nodes* operation had to be performed to connect meshes of the two regions properly.

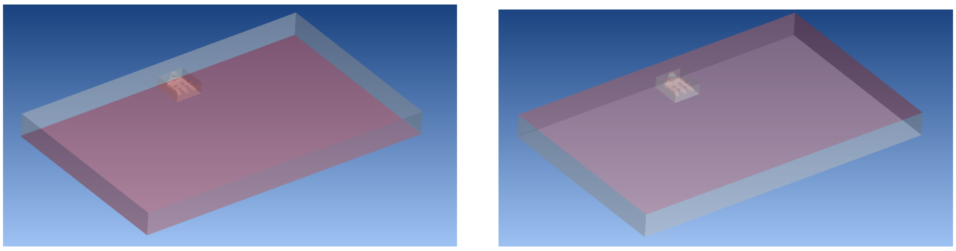

Fig. 3.8: Removed element sets (in red): floor and truck's downside

3.1.2 Direct Frequency Response analysis

Once the topology was made, the *Automatic domain creation* option allowed to transform the created volumes and surfaces into **domains** for the following analysis. The next step was to add in the *Data Tree Panel* a new analysis, in particular a *Direct Frequency Response (DFR)* analysis. A DFR analysis provides the response of a vibro-acoustic or aero-acoustic system to a specific excitation at a given frequency in physical coordinates [12]. In our case the aeroacoustic system response will be expressed in terms of propagation maps, that will be set as the output of the acoustic analysis indeed.
The first DFR analysis option is to specify the computational frequencies of the analysis, that is the **frequency range** for which the acoustic analysis has to be performed. However, here it was only specified the file name from which frequencies would have been read after source generation process (*sources_freq.nff*) and the maximum frequency computed (2000 Hz). In fact, for this type of analysis, the setting of the frequency range pertains to the iCFD utility. We'll see this procedure in the next section.
After that, the acoustic analysis **components** were added. The first one was the *Finite Fluid component*: it is the standard component used for modelling all types of finite acoustic media, points to an acoustic *fluid material* and is supported by a specific domain [13]. In our case the fluid material was ***air*** with standard properties: $c = 340\ m/s,\ \rho = 1.225\ kg/m^3$. Next to this, it is easy to say that, for this problem, domains to be assigned to Finite Fluid component were the source volume and the propagation volume. Moreover, the default boundary conditions on the free faces of a Finite Fluid component are rigid walls, that means normal velocity is equal to zero and the acoustic waves are perfectly reflected on those faces [13]. That is the reason why we deleted upper and lower surfaces in the topology: here floor and truck's downside are correctly simulated because of the default boudary conditions,

therefore such surfaces are useless in the analysis.
The second component was the *Infinite Fluid component*: it is used to model unbounded acoustic domains in free field radiation problems, is supported by 2D elements applied to the exterior boundary of the finite element domain and acts as a non-reflective boundary condition [13]. Therefore in the analysis it must be supported by a convex 2D domain and, as the Finite Fluid component, must point to a valid acoustic *fluid material*. Also in this case, ***air*** was set as fluid material, while lateral boundaries of the propagation region (fig. 3.9) were assigned to the component, as they are the only sides not in contact with any physical walls. Beside this options, Infinite Fluid component has two more properties to set: the *interpolation order* and the *reference coordinate system*. The first one represents the order N of the truncated multipole expansion used to approximate the pressure in far field. According to this formulation, pressure at distance r can be retrieved as:

$$p(r) = \frac{A_1}{r} + \frac{A_2}{r^2} + ... + \frac{A_N}{r^N}$$

The reference coordinate system is the infinite elements reference system and is characterized by the axes and the center. About the axes, the spherical system represents the best choice in most of cases, while the center is usually located in the middle of the finite elements domain for a symmetrical free field propagation. Despite this, in the analysis we considered for the center position the coordinates of the intersection point between diffusor's vertical axis and the upper surface. Tables 3.2 and 3.3 summarize the values of the chosen parameters for the Finite and the Infinite Fluid component.

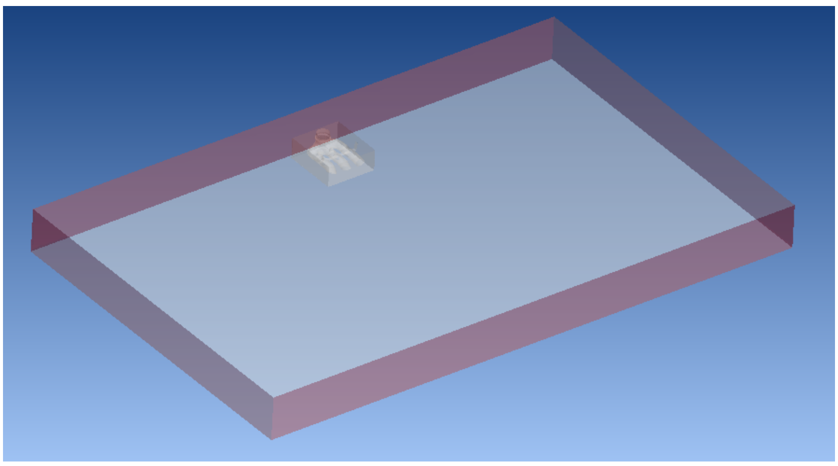

Fig. 3.9: Infinite Fluid component domain (in red)

Acoustic fluid material	*air* (standard properties)
Assigned domain	source and propagation regions

Tab. 3.2: Finite Fluid Component properties

Acoustic fluid material	*air* (standard properties)
Interpolation order	8
Reference coordinate system center	$[0, 0.284, -0.303]$
Reference coordinate system axes	spherical: $[1, 0, 0]$ $[0, 1, 0]$ $[0, 0, 1]$
Assigned domain	lateral boundaries

Tab. 3.3: Infinite Fluid Component properties

The next step was the addition of the **boundary condition**, in particular a *Lighthill volume boundary condition*. This one belongs to the aero-acoustics type and derives from the *Lighthill analogy* formulation, where is possible to obtain a wave propagation equation, with a source term at right-hand side, rearranging Navier-Stokes equations. Such term includes two differents type of sources: volume source and surface source. The first one, the Volume Source Term (see equation 1.1 for its expression), is related to turbulent noise and has a “hybrid” nature, meaning that it is computed by ACTRAN basing on CFD solution on the CFD mesh, and then results are mapped on the acoustic mesh. Therefore, its function is to compute acoustic sources basing on incompressible CFD analysis results [14]. Then the first parameter to set for *Lighthill volume boundary condition* was the file name where sources distribution in frequency domain would have been output from iCFD analysis (*sources_freq.nff* in our case). The next was the *filter amplitude* parameter, used to prevent source truncation due to CFD boundary conditions. It mostly depends on the mesh size and on domain extension: 0.05 has been chosen as value. The last was the domain assignment: source region was the selected option, according to the domains definition.
Finally, post-processing components were added to the analysis: three **virtual microphones** were created using *Points* tool and added to a different topology. Microphones position is shown in fig. 3.10. They will be used to show the trend of Sound Pressure Level (SPL) over frequency during post-processing. Then an **output map** was created in order to visualize pressure distribution on the whole model: for this reason *All* domain was assigned to this component. It was also specified the name of the output file (*maps.nff*) and set 1 for the step option to export results on every frequency.

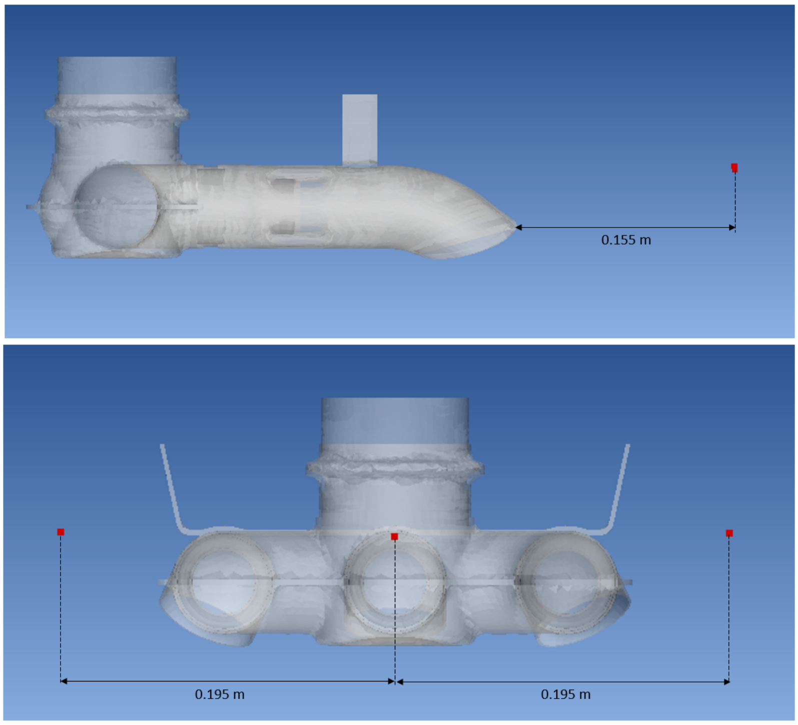

Fig. 3.10: Position of virtual microphones (in red)

3.1.3 iCFD analysis

We have already mentioned that by ACTRAN is possible to reconstruct acoustic sources starting from CFD results: this task is accomplished by the *iCFD analysis*. In general, iCFD is an ACTRAN utility that allows for the processing of CFD results for creating aero-acoustic sources or mapping mean flows. We added such analysis in a new ACTRAN page, in the *Data Tree Panel*. After that, as we wanted to use **SNGR** method to map the sources, we selected *SNGR component* in the analysis window. Here a number of parameters for reading the iCFD input file were set: STAR-CCM+ as the input CFD file format, *BDxx_steady_state.ccm* as the input CFD file name, *NFF* as the output file format, *sources_freq.nff* as the output file name (it is the same as the one provided in the Lighthill Volume boundary condition!) and the ACTRAN analysis file name, containing the acoustic mesh. *BDxx* denotes the two different meshes adopted in CFD analysis: *BD12* and *BD02* (see CFD results section for mesh comparison).

Then it was the turn of the parameters for computing the sources on the acoustic mesh: *RELATIVE* was set for *turbulence threshold method* and *K-Epsilon* for the *turbulence model.* **Turbulence threshold** gives indication of how many turbulent contributions are accounted for in the sources reconstruction process: increasing this quantity means to neglect more and more turbulent structures. About this, it was decided to set three different cases: the first one with 10%, the second one with 25% and the third one with 5% of turbulence threshold. Obiouvsly the chosen values are a compromise between the accuracy of solution and the computational time.
The **number of samples** is related to the stochastic process of synthesizing the turbulent velocity field in SNGR approach: in particular, each sample corresponds to a single number of the random generator. The integration of these samples on the acoustic domain during post-processing will give the correct results in terms of distribution and propagation maps. Also this parameter is related to the computational cost, since increasing the number of samples will raise the computational time, as well as the accuracy of the results. Also in this case, different options were considered: 1 sample and 10 samples. The first choice may seem too cheap, but the only way to realize movies showing the acoustic propagation in ACTRAN is to consider a single loadcase, i.e. a single sample.
The **number of turbulent modes** corresponds to the wave numbers selected in the velocity field spectrum, that is the spectrum where Turbulent Kinetic Energy (TKE) is extracted for the velocity field construction. Here 15 modes were initially set, but then the number was increased to 30.
As we said in the previous section, the **frequency range** was set in iCFD analysis. We added a frequency domain as a sub-branch of SNGR component and set the frequencies of the analysis. We considered two cases with 400 Hz as min value and 2000 Hz as max value: the first one with step 400 Hz and the second one with step 100 Hz. So the first range included only five frequencies (400, 800, 1200, 1600 and 2000 Hz), while the other one seventeen frequencies. The latter case is more expensive in terms of computational time, but gives more realistic results when plotting SPL over frequency. The last operation was to add a second SNGR component sub-branch, the **Turbulence Spectrum**, where turbulent energy is extracted basing on chosen turbulent modes. Here it was decided to mantain the default option, that is *Von Karman - Pao* type.
After that, the analysis was exported and then launched. iCFD analysis main result is the *sources_freq.nff* file, which contains the distribution of computed sources in frequency domain. Source distributions for the considered cases may be visualized in ACTRANVI *Render Window*, as we did in post-processing. The generated file is then used as input of the acoustic analysis previously set, that is launched after the iCFD.

3.1.4 Post-processing and results

Let us first visualize the **maps of sources distribution**, output of iCFD analysis. In particular, we will show the comparison between 1 sample and 10 samples (with maps showing mean on all samples) and then between BD02 and BD12. For each case we will consider two frequencies (800 Hz and 1200 Hz), 30 turbulent modes and 10% as turbulence threshold. Maps views are on xy and yz planes.

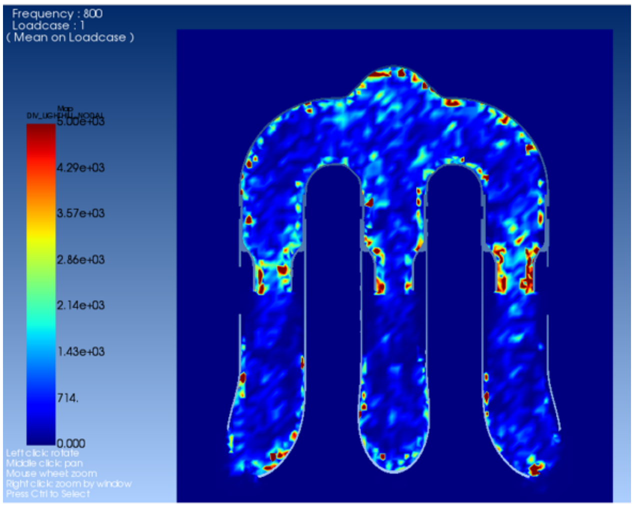

Fig. 3.11: $f = 800\ Hz$, 1 sample, BD12, xy plane

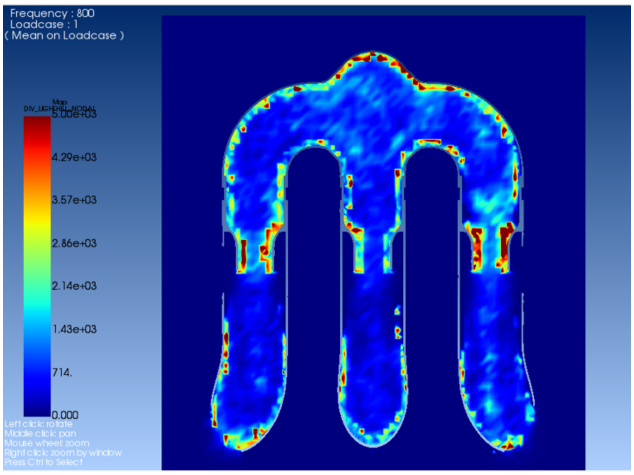

Fig. 3.12: $f = 800\ Hz$, 10 samples, BD12, xy plane

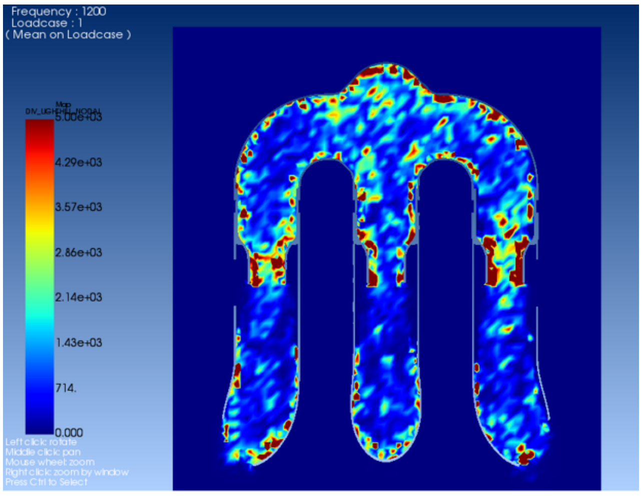

Fig. 3.13: $f = 1200\ Hz$, 1 sample, BD12, xy plane

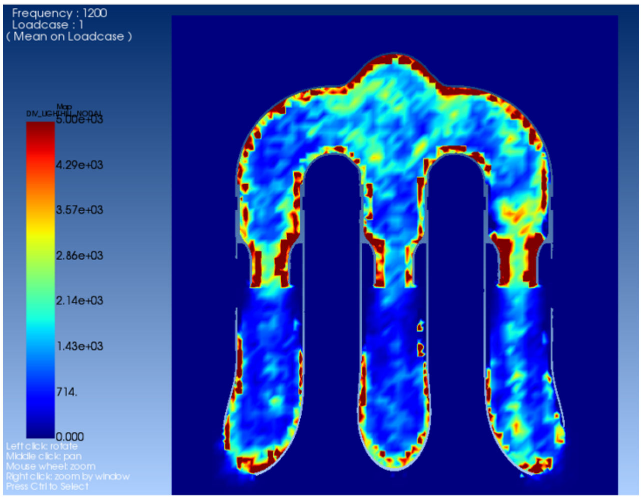

Fig. 3.14: $f = 1200\ Hz$, 10 samples, BD12, xy plane

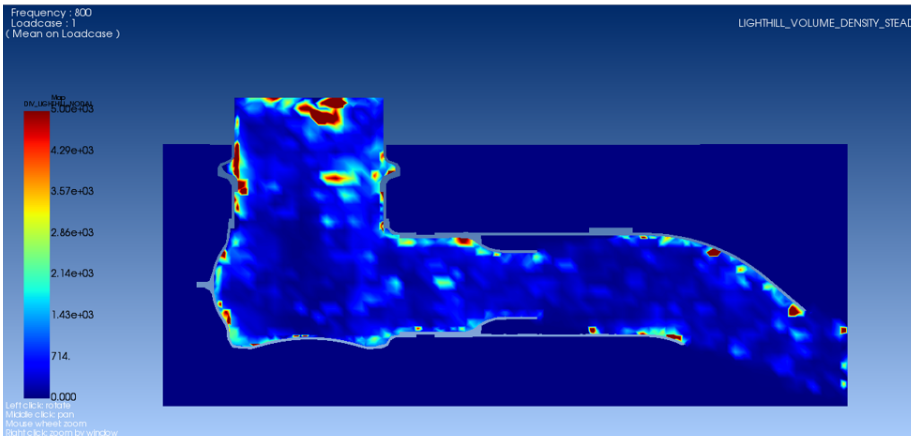

Fig. 3.15: $f = 800\ Hz$, 10 samples, BD02, yz plane

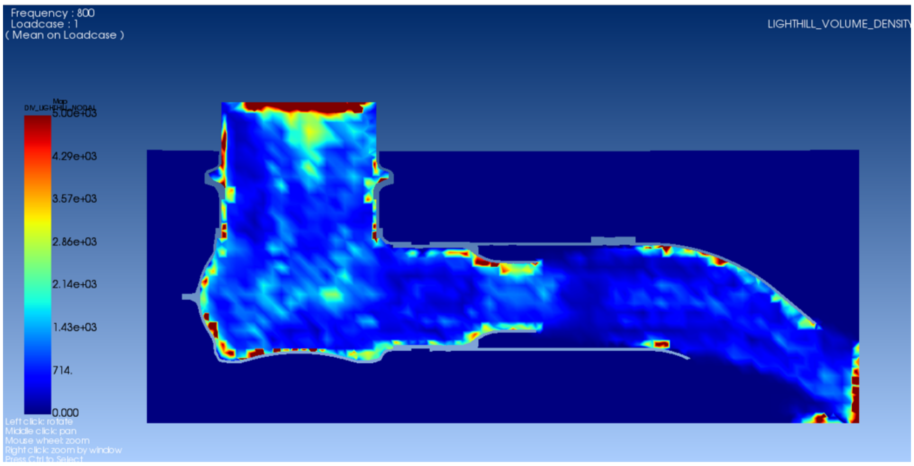

Fig. 3.16: $f = 800\ Hz$, 10 samples, BD12, yz plane

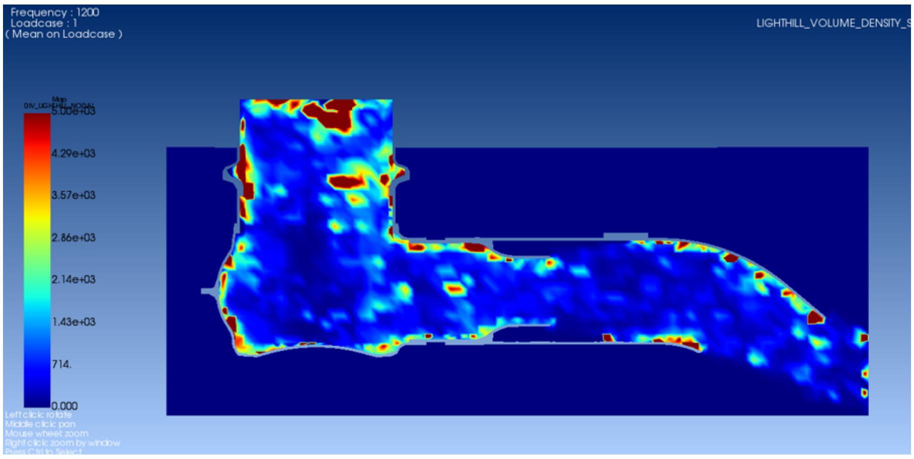

Fig. 3.17: $f = 1200\ Hz$, 10 samples, BD02, yz plane

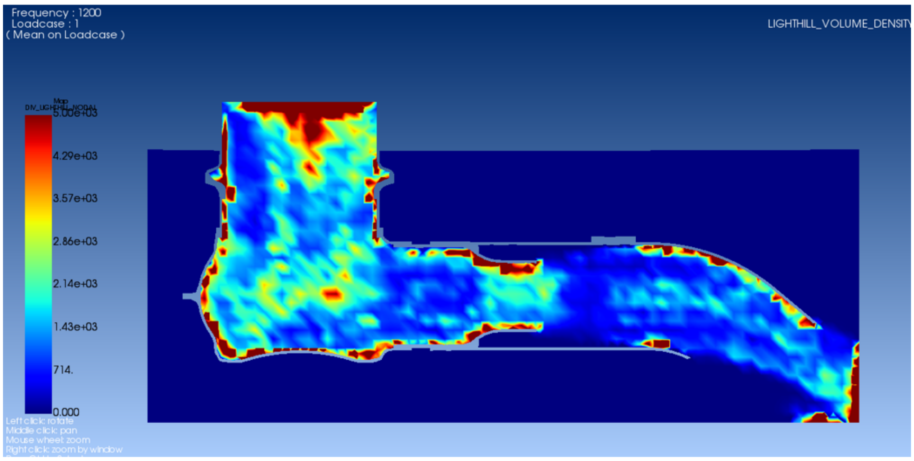

Fig. 3.18: $f = 1200\ Hz$, 10 samples, BD12, yz plane

In the following the **pressure maps** obtained through Direct Frequency Response analysis are shown to visualize the acoustic propagation. We will consider the corresponding cases of source distribution maps, with 30 turbulent modes and 10% turbulence threshold as well.

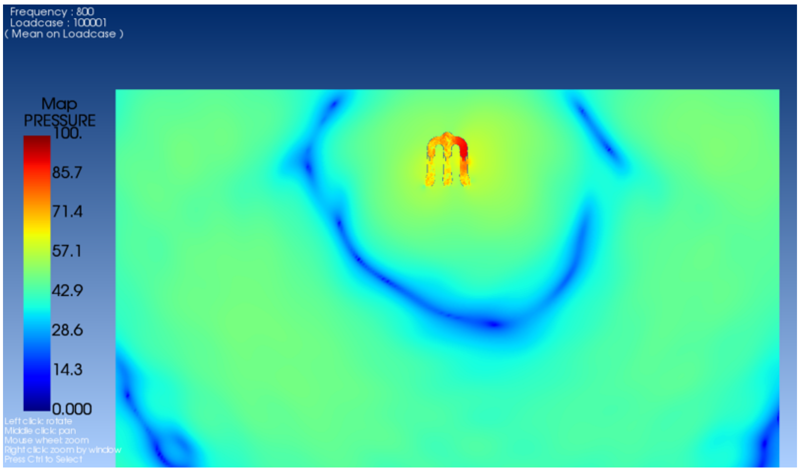

Fig. 3.19: $f = 800\ Hz$, 1 sample, BD12, xy plane

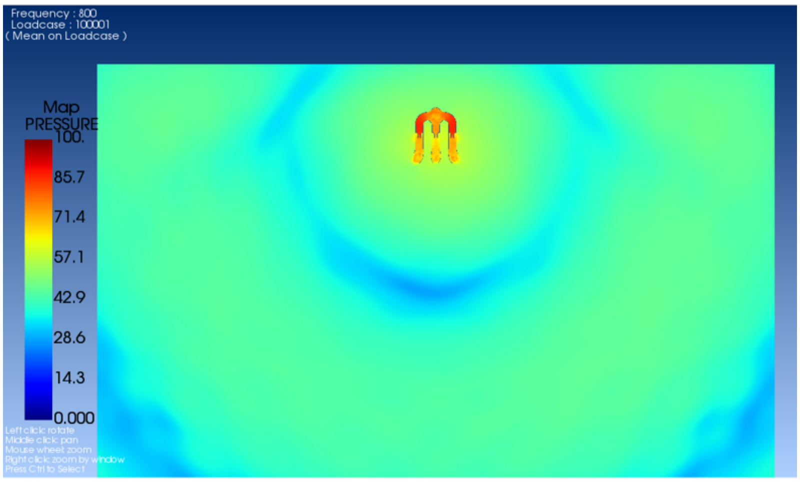

Fig. 3.20: $f = 800\ Hz$, 10 samples, BD12, xy plane

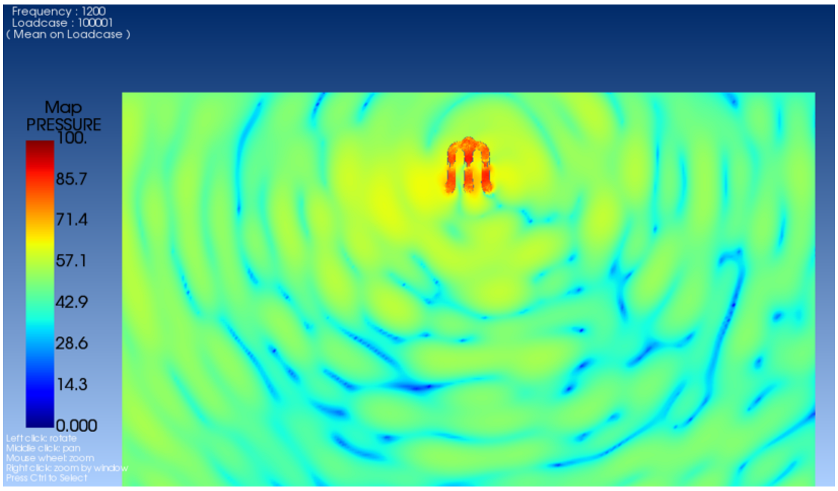

Fig. 3.21: $f = 1200\ Hz$, 1 sample, BD12, xy plane

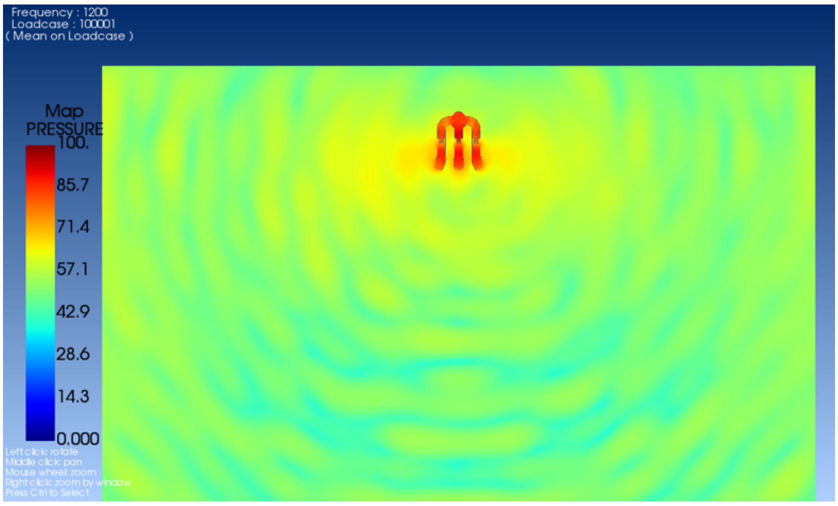

Fig. 3.22: $f = 1200\ Hz$, 10 samples, BD12, xy plane

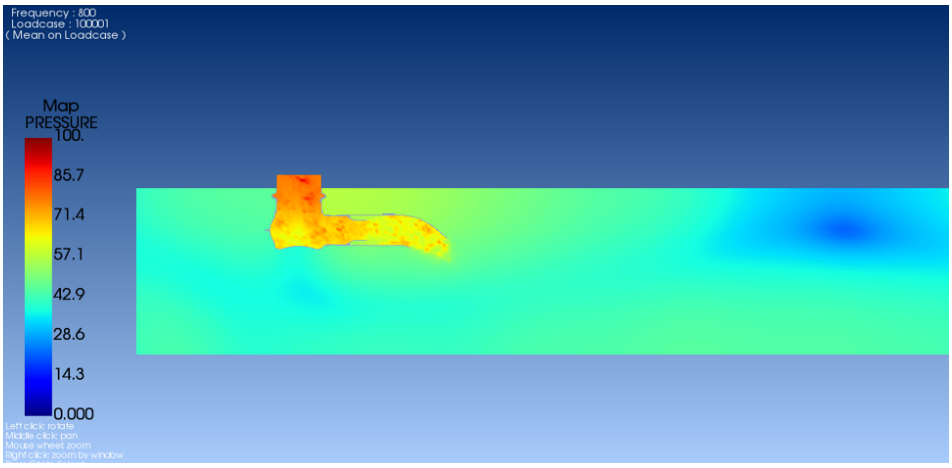

Fig. 3.23: $f = 800\ Hz$, 10 samples, BD02, yz plane

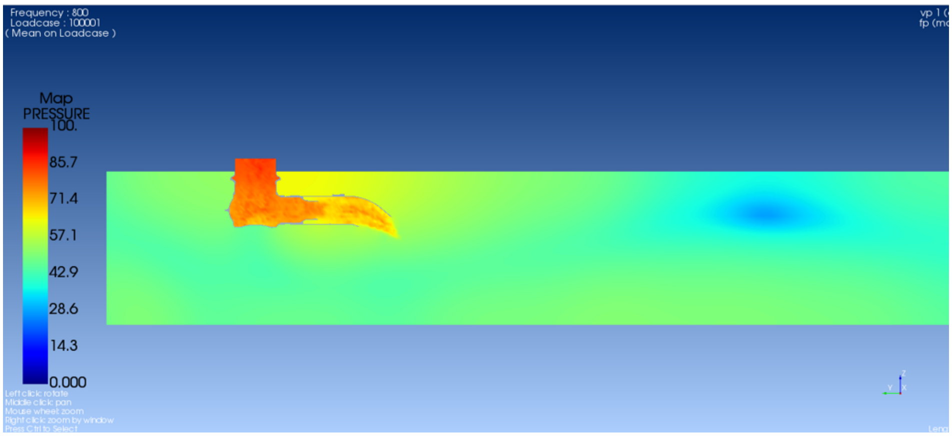

Fig. 3.24: $f = 800\ Hz$, 10 samples, BD12, yz plane

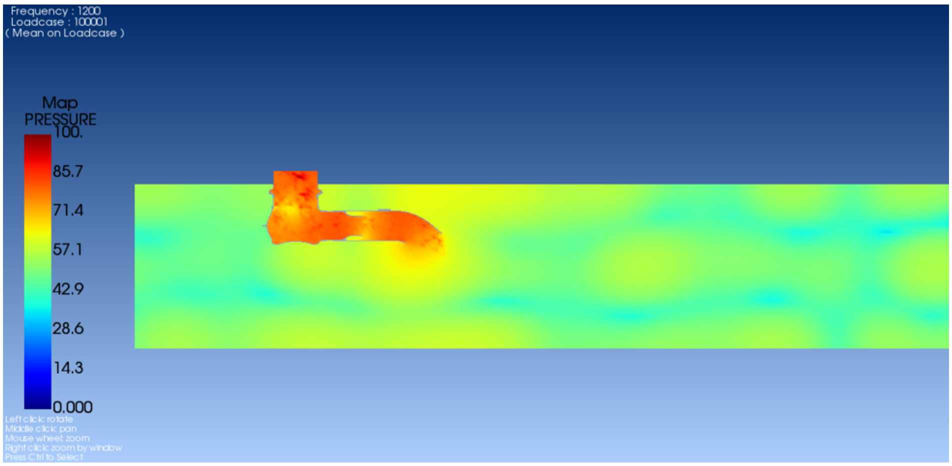

Fig. 3.25: $f = 1200\ Hz$, 10 samples, BD02, yz plane

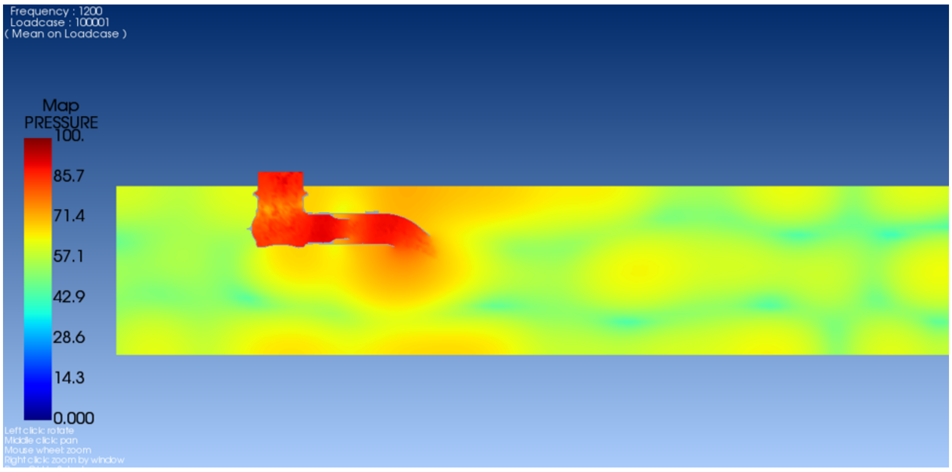

Fig. 3.26: $f = 1200\ Hz$, 10 samples, BD12, yz plane

Finally we have the plot of **Sound Pressure Level at microphones**. In each diagram is reported the SPL trend over frequency at left/center/right microphone in different conditions, that is with different values of the analysis parameters. In some cases five frequencies will be considered, corresponding to the case of 400 Hz as frequency step in the analysis, but most of the diagrams will refer to the case of 100 Hz as frequency step for a better comparison with SPL plots coming from the CFD analysis.

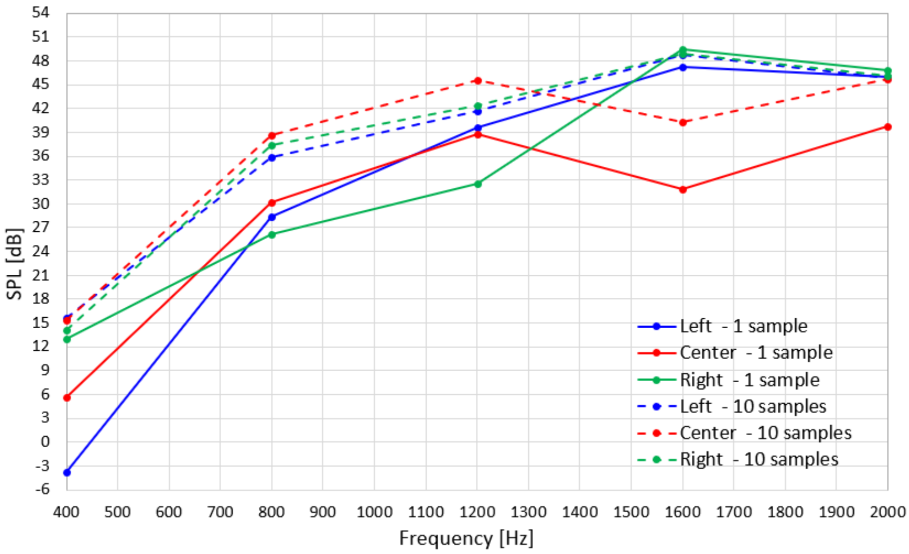

Fig. 3.27: SPL at microphones: comparison between 1 sample and 10 samples (10% turbulence threshold, 15 turbulent modes)

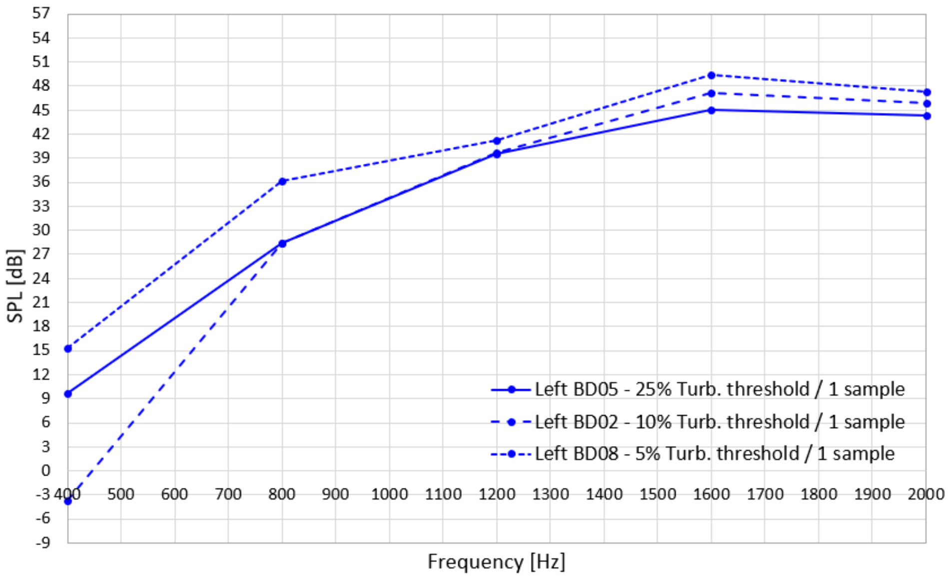

Fig. 3.28: SPL at left microphone: comparison between 5%, 10% and 25% of turbulence threshold (1 sample, 15 turbulent modes)

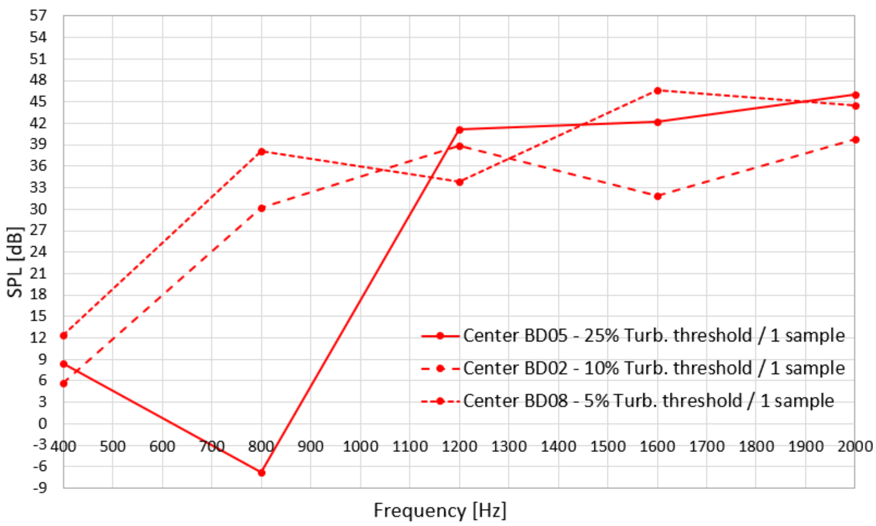

Fig. 3.29: SPL at central microphone: comparison between 5%, 10% and 25% of turbulence threshold (1 sample, 15 turbulent modes)

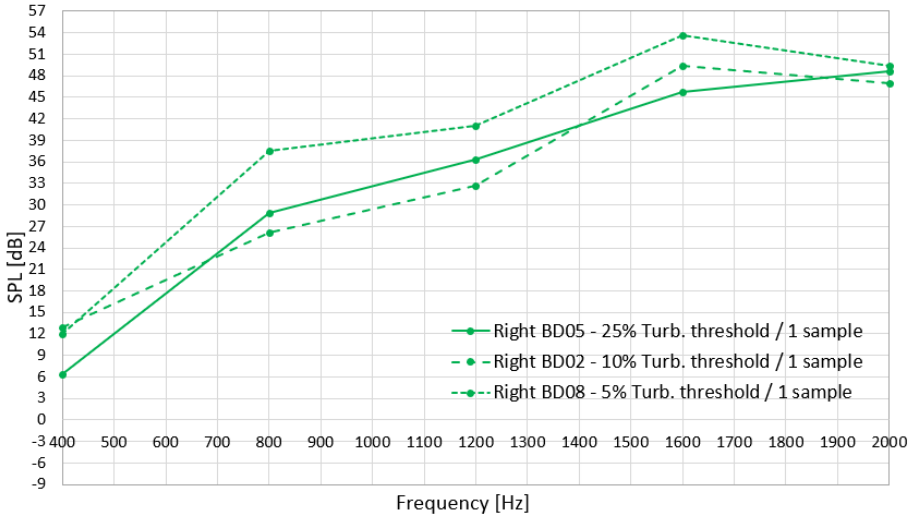

Fig. 3.30: SPL at right microphone: comparison between 5%, 10% and 25% of turbulence threshold (1 sample, 15 turbulent modes)

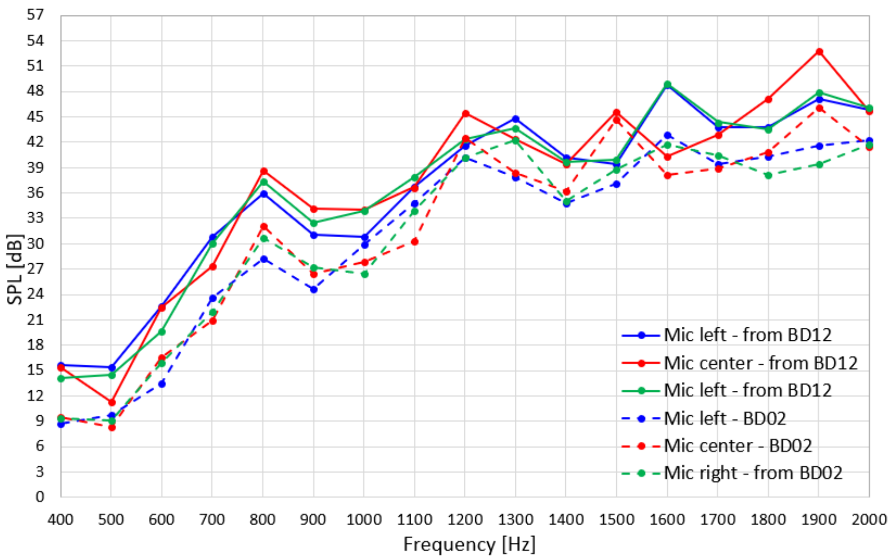

Fig. 3.31: SPL at microphones: comparison between BD02 and BD12 (10 samples, 10% turbulence threshold)

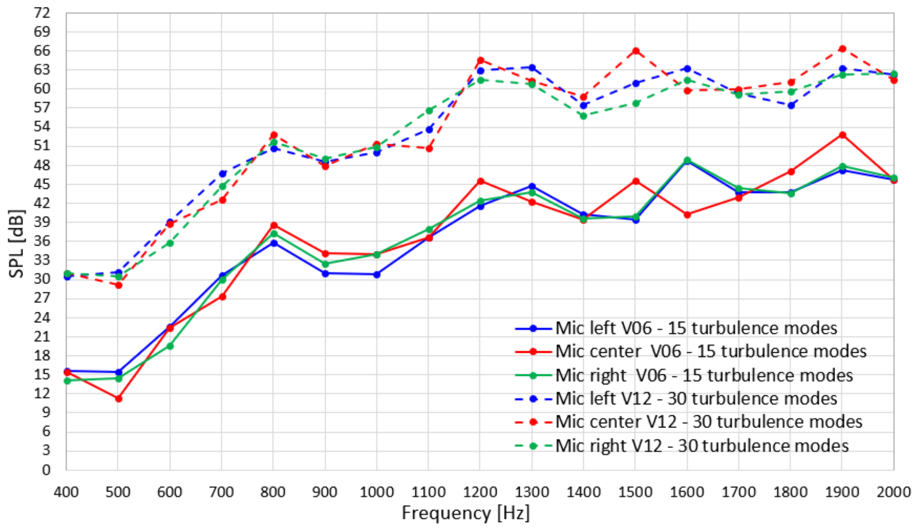

Fig. 3.32: SPL at microphones: comparison between 15 and 30 turbulent modes (10 samples, 10% turbulence threshold)

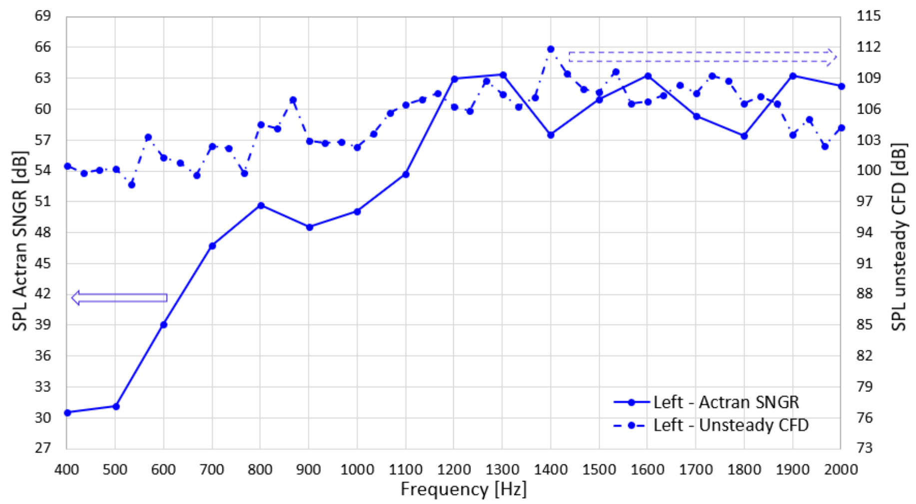

Fig. 3.33: SPL at left microphone: comparison between results from Actran SNGR and from unsteady CFD (10 samples, 10% turbulence threshold, 30 turbulent modes)

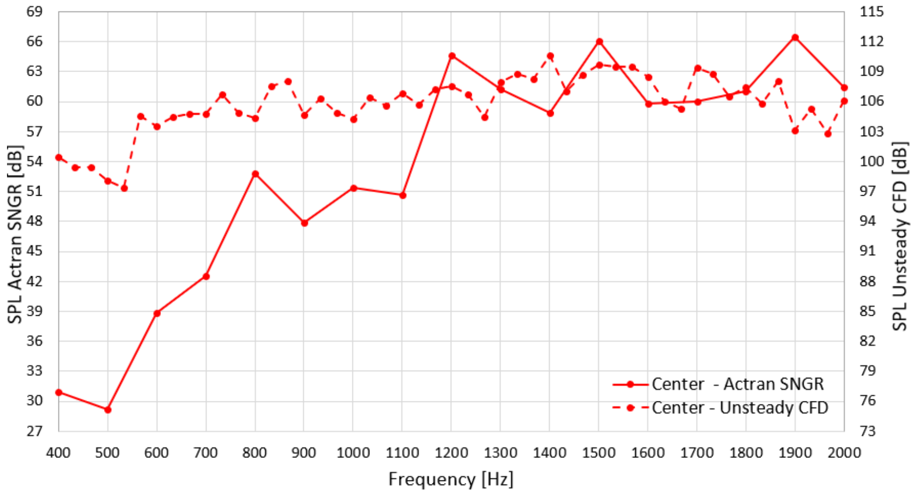

Fig. 3.34: SPL at central microphone: comparison between results from Actran SNGR and from unsteady CFD (10 samples, 10% turbulence threshold, 30 turbulent modes)

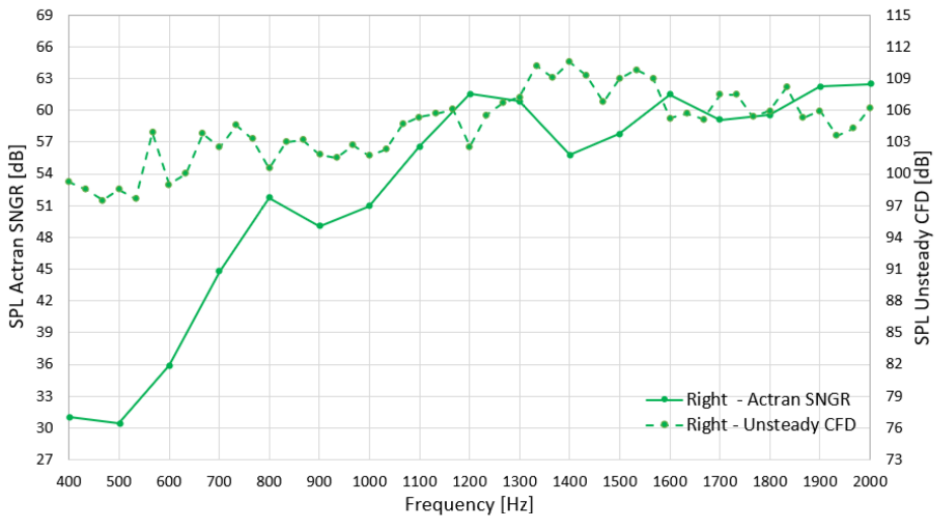

Fig. 3.35: SPL at right microphone: comparison between results from Actran SNGR and from unsteady CFD (10 samples, 10% turbulence threshold, 30 turbulent modes)

3.2 Perforated plate design

Moving to the perforated plate configuration, the same steps were repeated for the analysis set-up. Also in this case the geometry of the diffusor was imported in ACTRAN and then re-meshed with a 0.005 m element-sized mesh (figure 3.36). At first such element dimension seemed inappropriate for the perforated plate because of its 4 mm diameter holes, and for this reason 0.002 m was the initial choice for the diffusor surface and source region element size. However memory issues when launching the analysis led to take 5 mm as element size also for this case, at the same time avoiding a bad resolution of the mesh around the perforated plate (figure 3.37).

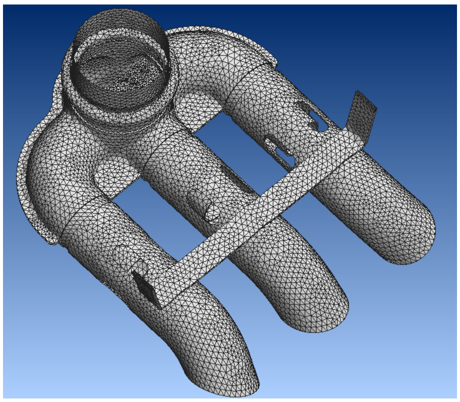

Fig. 3.36: Re-meshed diffusor (perforated plate configuration)

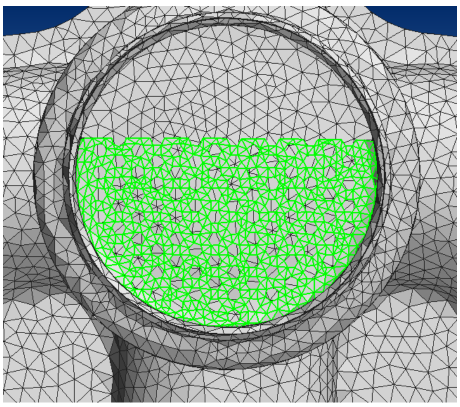

Fig. 3.37: Mesh detail on the perforated plate

The geometry of the source and propagation region is the same as in baseline configuration (fig. 3.38), and also 3D elements of the created volume mesh have the same dimension (see table 3.4).

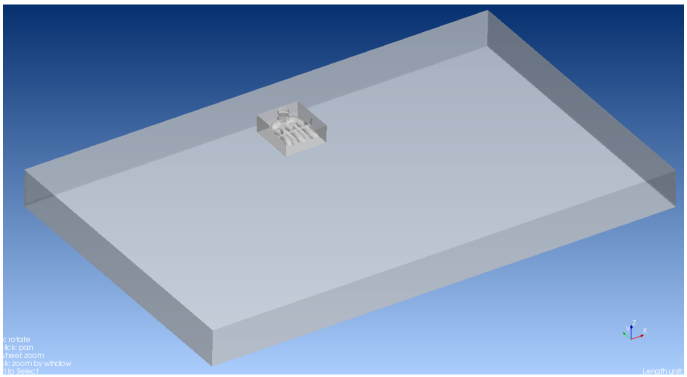

Fig. 3.38: Topology for perforated plate design

Source region	0.005 m
Propagation region	0.015 m

Tab. 3.4: Mesh elements size for perforated plate design

Once the topology was created, the setting of the acoustic analysis and iCFD analysis was identical to the one already made for baseline design case. For this reason, we do not report again all parameters options and related explanations, but only set values that differ from the previous configuration.
Basing on the sensitivity analysis of parameters carried out for baseline design, in the acoustic analysis were considered both 400 and 100 as step option for *frequency range* (min frequency: 400 Hz, max frequency: 2000 Hz), 10% of *turbulence threshold*, 10 *samples*, 15/30 *turbulent modes* and both PP02 and PP12 for input file CFD volume mesh. Results in terms of source distribution, pressure maps and SPL-frequency plot at microphones for perforated plate case are shown in the following section.

3.2.1 Post-processing and results

For the perforated plate design, we only show maps and diagrams of the final model, after the sensitivity on the analysis parameters. This turned out to be characterized by 10 samples, 30 turbulent modes, 10% as turbulence threshold and PP12 as input CFD mesh. For the **sources distribution maps** and the **pressure maps** we'll consider the same medium frequencies of the baseline design case (800 Hz and 1200 Hz), but we will neglect comparisons between different number of samples and CFD mesh type.

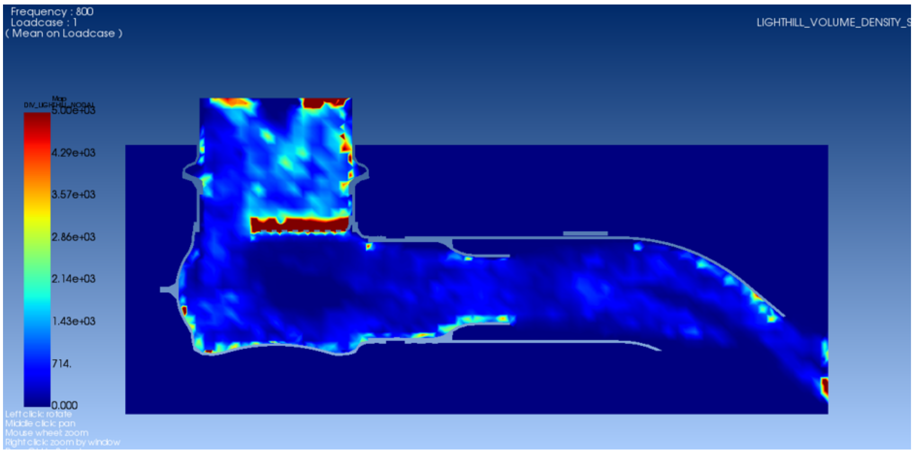

Fig. 3.39: Sources map: $f = 800\ Hz$, yz plane

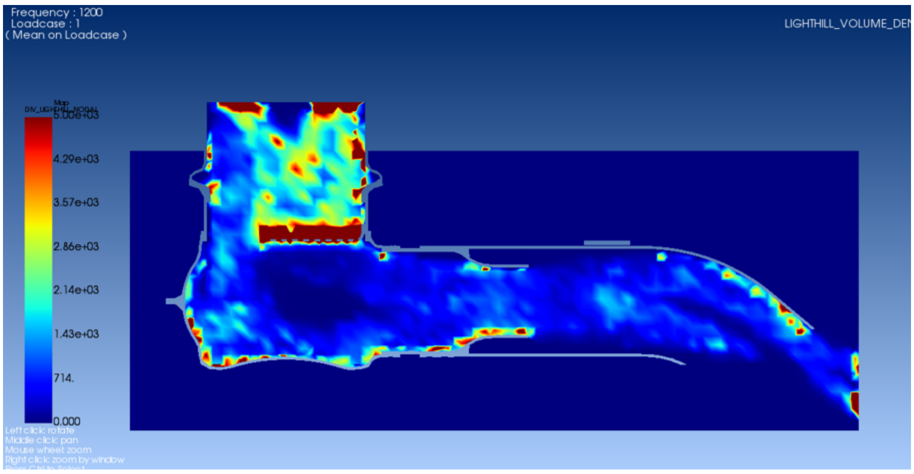

Fig. 3.40: Sources map: $f = 1200\ Hz$, yz plane

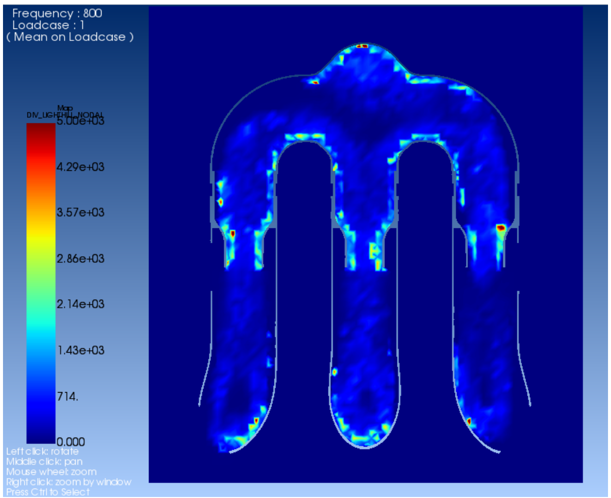

Fig. 3.41: Sources map: $f = 800\ Hz$, xy plane

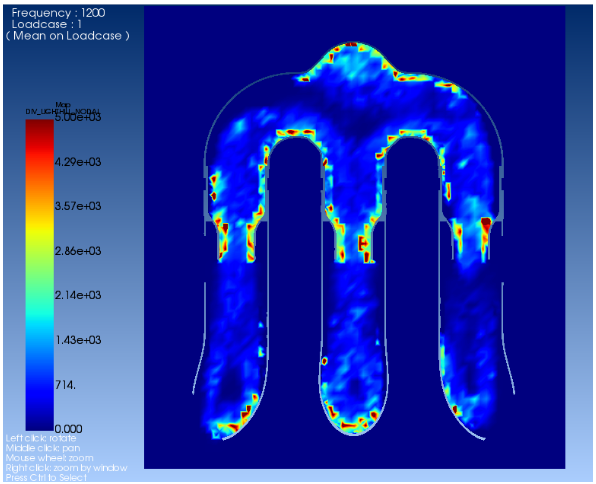

Fig. 3.42: Sources map: $f = 1200\ Hz$, xy plane

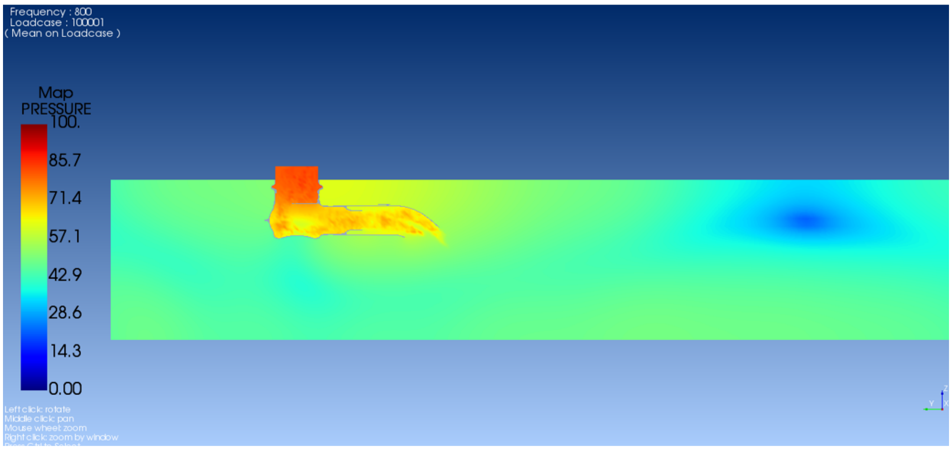

Fig. 3.43: Pressure map: $f = 800\ Hz$, yz plane

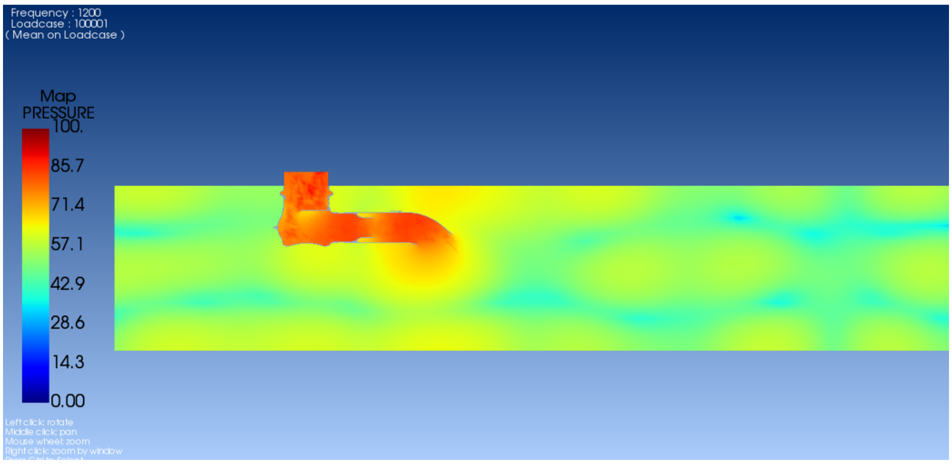

Fig. 3.44: Pressure map: $f = 1200\ Hz$, yz plane

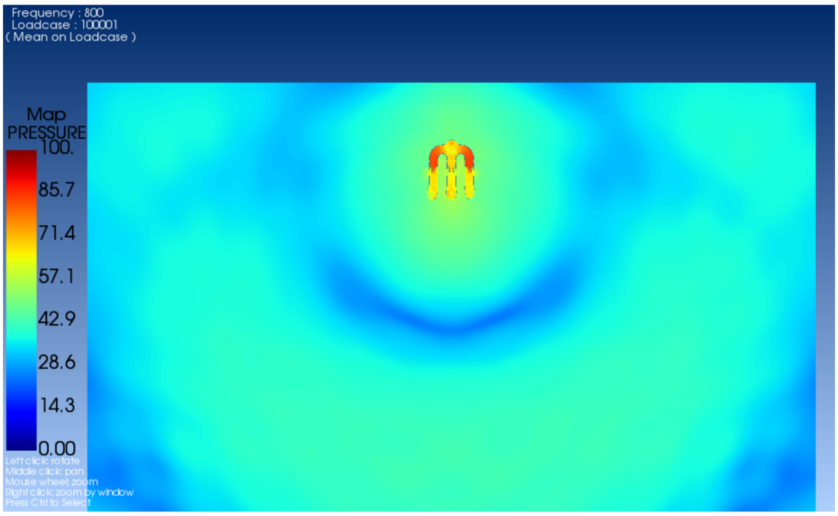

Fig. 3.45: Pressure map: $f = 800\ Hz$, xy plane

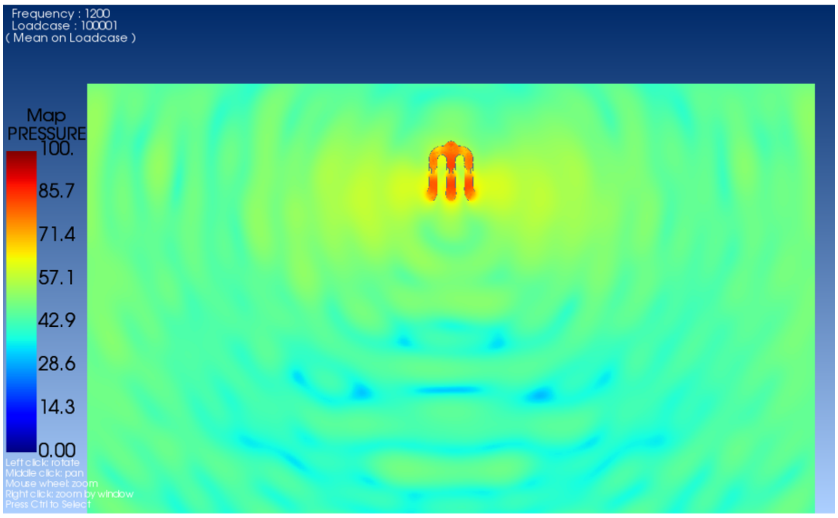

Fig. 3.46: Pressure map: $f = 1200\ Hz$, xy plane

In **SPL plot** at microphones for the perforated plate design, only two graphs are shown. The first one is simply a comparison between Sound Pressure Level with 15 turbulent modes and 30 turbulent modes in PP design, while the second one is the final confrontation of SPL values between the two designs, baseline and perforated plate, in the frequency range considered.

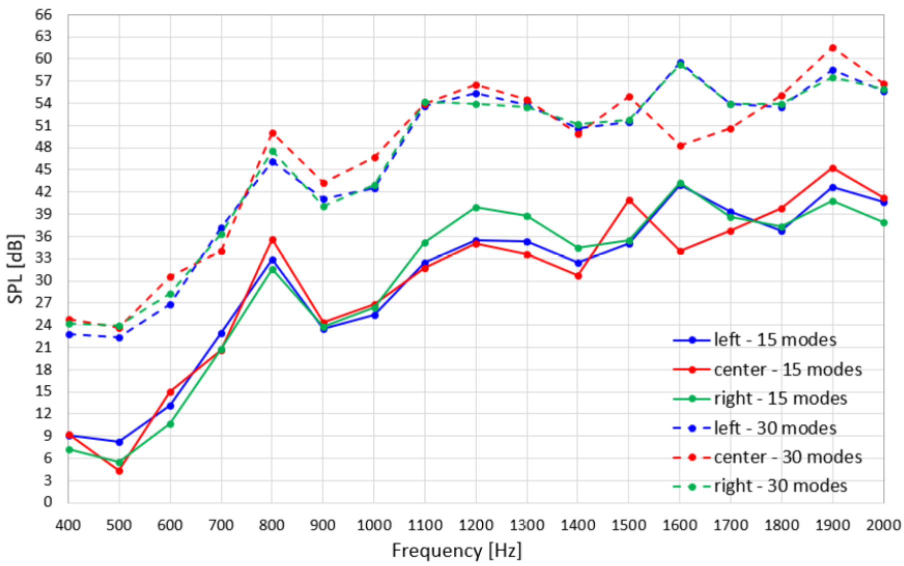

Fig. 3.47: SPL at microphones: 15 vs 30 turbulent modes (10 samples, 10% turbulence threshold)

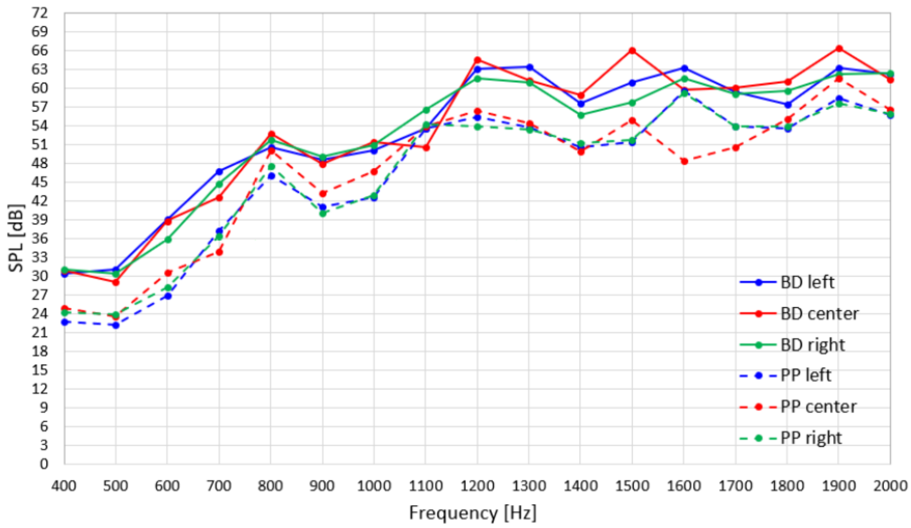

Fig. 3.48: SPL at microphones: baseline design vs perforated plate design (10 samples, 10% turbulence threshold, 30 turbulent modes)

4. DISCUSSION OF THE RESULTS

4.1 Sources distribution maps

Looking at the maps of reconstructed sources in xy and yz planes (figures 3.11 - 3.18 and 3.39 - 3.42), the first important characteristic to observe is the increase in the intensity of sources with frequency: in all considered cases the amplitude of the acoustic sources at 800 Hz is lower than it is at 1200 Hz in all parts of the diffusor. Obiouvsly, the red spots inside the maps identify the most intense acoustic sources, to which generally correspond the areas of the flow with the highest level of turbulence.
About the comparison between 1 sample and 10 samples (figures 3.11, 3.12, 3.13 and 3.14), it is possible to see a more regular distribution of sources in the latter case. This can be explained by the source reconstruction process adopted in SNGR method: taking into account more loadcases means to assign to the synthetic velocity field, and therefore to the source term in Lighthill formulation, more random characteristics typical of turbulent flows. From this point of view, when using SNGR approach for aeroacoustic excitations within an acoustic propagation problem, it is always a better option to consider a certain number of samples. Nevertheless, in some situations may be useful to set a single loadcase in the analysis, for example when a quick calculation is required during the early stages of the simulation.
The comparison between sources maps from BD02 and BD12 (figures 3.15, 3.16, 3.17 and 3.18) puts in evidence the effect of considering a different size of the elements of CFD mesh. In both cases, we can observe higher values of sources amplitude near the walls and at the inlet on the top of the diffusor. Despite some similarities in the distribution, overall results show higher intensity of sources for BD12 rather than BD02, though.
However, the most important result for this section is revealed by the direct comparison between the baseline design and the perforated plate design in terms of acoustic sources. Comparing views in yz plane at both frequencies (figures 3.16 - 3.18 and 3.39 - 3.40), it is clearly visible the drastic reduction in intensity of the acoustic sources downstream of the perforated plate. Therefore, the insertion of the perforated plate appears to be an effective method for reducing the aerodynamic noise generated by the exhaust system. Views in xy plane confirm this result: values in PP configuration are lower than in BD, because the position of the viewing plane is located below the perforated plate.

4.2 Pressure maps

In the pressure maps (figures 3.19 - 3.26 and 3.43 - 3.46) we can observe the propagation of the acoustic signal, originating from sources in the diffusor, throughout the whole domain. More precisely, the mapped quantity represents the amplitude of the pressure wave in dB. The comparison between these maps for the different cases considered is the same as that already done for source distribution maps. In fact, we can see a correspondence in terms of values between the intensity of the sources and the amplitude of the pressure signal within the acoustic field. Therefore, on this aspect, the pressure maps can be explained referring to the previous section. About the acoustic propagation pattern, we can clearly see the presence of the *propagation modes* at the frequency of 1200 Hz (figure 3.25 and 3.26), while they are less noticeable at 800 Hz. Moreover, at 1200 Hz it is possible to better observe on yz plane the significant noise reduction at the diffusor outlet due to the switch to the perforated plate configuration (see figures 3.26 and 3.44).

4.3 Sound Pressure Level at microphones

In all graphs shown (figures 3.27 - 3.35, 3.47 and 3.48), the Sound Pressure Level is characterized by a quite fast growth at low frequencies and by a slower increase at high frequencies, where SPL values describe an almost flat trend. This happens both considering the range with five frequencies ([400:400:2000] Hz) and with seventeen frequencies ([400:100:2000] Hz).
About the comparison between a single loadcase and multiple loadcases (fig. 3.27), SPL values at each microphone are greater in the second case for all considered frequencies, according with the intensity levels of the sources.
Certainly more interesting are the SPL curves at left, central and right microphone with different values of turbulence threshold set during the optimization of the analysis parameters (figures 3.28, 3.29 and 3.30). Beside a general reduction of SPL when raising the threshold up, in some cases it is possible to notice falls in SPL values when referring to the case of 25% (see fig. 3.29). In fact, as we have already mentioned, increasing the turbulence threshold means to neglect more turbulent contributions to noise sources, to the advantage of a saving in computational resources; therefore such behavior can be explained with lacks in considered turbulent structures.
Moving to the graph where BD02-BD12 confrontation is shown (figure 3.31), we can say that SPL trend over frequency is maintained between the two cases, even if values are lower for BD02. This result totally agrees with the corresponding maps. Even changing the number of turbulent modes doesn't affect the shape of the solution much in SPL curves, as shown in figures 3.32 for baseline design and 3.47 for perforated plate. The main difference is the

flattening of the SPL trends between 1200 Hz and 2000 Hz when switching from 15 to 30 modes. In addition to this, 30 modes case is characterized by higher Sound Pressure Levels than 15 modes because of a greater number of frequencies used for turbulent velocity synthesis in SNGR method.
Anyway, the first important result is the comparison in terms of SPL at microphones between Actran SNGR and unsteady CFD simulation (figures 3.33, 3.34 and 3.35). Since SPL values obtained through SNGR method are *relative*, we have to apply a scale factor to compare them with absolute values from unsteady CFD. Applying a scale factor between the two sets of values practically means to translate the curve with results of SNGR upwards by a certain quantity of dB, that is the same for all microphones. The translation doesn't change the shape of the curve, so we are able to compare the two trends. In the figures mentioned above, the dB scale on the left refers to Actran SNGR values, while the dB scale on the right refers to SPLs from unsteady CFD. The accordance between the two analysis takes place at high frequencies, approximately above 1200 Hz. Below this frequency, SPL values from Actran SNGR and unsteady CFD differ significantly.
The second important result is shown in figure 3.48, where SPL for baseline design and for perforated plate design are compared. We can observe a reduction of SPL at microphones for perforated plate configuration as a consequence of reduced turbulent noise outcoming from the diffusor. Such a result also confirms the effectiveness of the perforated plate device.

5. CONCLUSIONS

Results of ACTRAN analysis overall proved the utility of the perforated plate in reducing the noise of the exhaust system and, at the same time, turned out to be in good agreement with results of CFD analysis.
With respect to the first point, the insertion of the perforated plate to cover part of the diffuser inlet duct allowed a considerable reduction of the flow's turbulent structures and as a consequence of the intensity of the acoustic sources obtained using Stochastic Noise Generation and Radiation approach. The agreement with results of the unsteady CFD simulation has been verified, in particular, through the plot of Sound Pressure Level at microphones, where we could see a similar trend over 1200 Hz. Below such frequency, the differentiation between the two curves in the graph may be attributable to three different factors: the approximation of the statistical-based SNGR method, the very high integration times that would be required in the unsteady CFD simulation to correctly describe the low frequencies and the assumption of considering in the unsteady CFD a continuous flow coming from the engine, and not pulsed as it is in reality. Low frequency components are in fact mainly due to flow pulsations, and neglecting them only means being more interested in high frequencies in aeroacoustic studies.
As expected, the two types of CFD mesh led to different results in terms of acoustic maps. A quick comparison with the corresponding TKE maps of CFD analysis reveals that high turbulent energy areas are not necessarily the noisiest ones. This may at first appear contradictory. Actually, the distribution and the amplitude of acoustic sources in SNGR method depend not only on turbulent kinetic energy, but also on velocity and dissipation rate, which together form the set of variables provided by the input steady CFD analysis. If we only focus on the results of the acoustic analysis, a possible explanation of higher intensity levels in source maps for *BD12* could be due to the characteristics of the mesh itself. From this point of view, sources amplitude and pressure signal are greater for finer mesh because smaller elements allows to account for more turbulent scales in the synthesis process of turbulent velocity field. For this reason, now we could say that *BD12/PP12* mesh represents the best choice to assign as input to the acoustic analysis.
Even if not all results related to the variation of the analysis parameters have been provided, the sensitivity on the variables involved in SNGR method allowed us to understand the influence of each of them on the final maps and diagrams. Ultimately, the hybrid scheme and the SNGR method imple-

mented in ACTRAN have provided reliable results in determining the noise generated by the truck's exhaust system, that was the goal of this study.

BIBLIOGRAPHY

[1] Stefan Schoder and Manfred Kaltenbacher. *Hybrid Aeroacoustic Computations: State of Art and New Achievements.* 11 February 2020.

[2] Michael Weitz. *An Approach to Compute Cavity Noise using Stochastic Noise Generation and Radiation.* Master's Thesis, Technische Universitat Wien, 2019.

[3] Alastair West and Mirela Caraeni. *Jet Noise Prediction using a Permeable FW-H Solver.* Conference Paper, June 2015.

[4] Anders Rynell, Mattias Chevalier, Mats Abom and Gunilla Efraimsson. *A numerical study of noise characteristics originating from a shrouded subsonic automotive fan.* Applied Acoustics journal, 2018 .

[5] Mélanie Piellard. *A hybrid method for Computational AeroAcoustics applied to confined geometries.* Thése pour le titre de docteur specialité acoustique, Ecole Centrale de Lyon, 27 November 2008.

[6] Simone Vizzini, Magnus Knutsson, Maria Dybeck and Mats Abom. *Flow Noise Generation in a Pipe Bend.* SAE Technical Paper, June 2018.

[7] C. Bailly, P. Lafon and S. Candel. *Computation of noise generation and propagation for free and confined turbulent flows.* AIAA and CEAS, Aeroacoustics Conference, State College, PA, May 6-8, 1996.

[8] Pavel Niedoba, Jaroslav Bajko, Miroslav Jícha and Libor Cêrmák. *Sensitivity analysis of source region size on results of Stochastic Noise Generation and Radiation model.* Inter Noise, Melbourne, 16-19 November 2014.

[9] *Introduction to meshing in ActranVI.* ActranVI - Theory 1, FFT.

[10] *Actran general organization.* Actran INTRO - Theory 3, FFT.

[11] *ActranVI meshing tools: Introduction to meshing tools functions.* Actran Training - VI, FFT.

[12] *Aeroacoustic study of an HVAC duct.* Actran aeroacoustics - Workshop 1, FFT.

[13] *Acoustic simulation.* Actran ACOUSTICS - Theory 1, FFT.

[14] *Introduction to aeroacoustics.* Actran aeroacoustics - Theory 1, FFT.